IEEE Access
Multidisciplinary ⋮ Rapid Review ⋮ Open Access Journal

Received 19 July 2024, accepted 12 August 2024, date of publication 15 August 2024, date of current version 28 August 2024.

Digital Object Identifier 10.1109/ACCESS.2024.3444054

RESEARCH ARTICLE

A Dynamic Multitarget Obstacle Tracking and Monitoring Method for Vehicle Routing Based on Multiple Constraint Composite Perception Association Filtering

GUOXIN HAN[1,2], FUYUN LIU[1], HUIQI LIU[1], JUCAI DENG[3], WEIHUA BAI[2], AND KEQIN LI[4], (Fellow, IEEE)

[1]College of Mechanical and Electrical Engineering, Guilin University of Electronic Technology, Guilin 541004, China
[2]College of Computer Science and Software, Zhaoqing University, Zhaoqing 526061, China
[3]Commercial Vehicle Technology Center, Dongfeng Liuzhou Automobile Company Ltd., Liuzhou 545116, China
[4]Department of Computer Science, State University of New York at New Paltz, New Paltz, NY 12561, USA

Corresponding author: Fuyun Liu (liufuyun310@aliyun.com)

This work was supported in part by Guangxi Key Research and Development Project, China, under Grant GuiKeAB23026106; in part by Zhaoqing University Research Fund Project, China, under Grant QN202333; and in part by Guangdong Provincial University Key Scientific Research Project, China, under Grant 2020ZDZX3020.

ABSTRACT Multitarget tracking technology is the core topic in the field of intelligent driving. Multi-target complex manoeuvring, measurement outliers and unknown environmental prior parameters strongly affect the tracking accuracy of the target state. To address the accurate tracking of multitarget under the above complex working conditions, we propose a new multitarget tracking algorithm, named the Multiconstrained Generalized Probabilistic Data Association Filtering (MCGPDAF) algorithm. In this algorithm, we use the target position and heading information to construct constraint parameters to calculate the association probability between each effective measurement combination and the target track. This algorithm can effectively suppress the measurement association anomalies and aprior information errors, as well as enable the robust association of single-sensor multitarget measurements and accurate tracking of target states under complex working conditions. On this basis, a multitarget tracking method based on composite perception fusion is further constructed, and the correlation sequential track association algorithm and covariance cross fusion algorithm are used to enable the track association and the estimation and fusion of target states among multiple sensors, which further enhances the tracking accuracy of the multitarget state. The simulation and real vehicle experiment results reveal that, compared to current advanced algorithms, the RMSE and MAPE of the MCGPDAF algorithm for multitarget tracking are enhanced by an average of 23.97% and 24.35%, respectively. Additionally, the MOTA and MOTP of the MCGPDAF algorithm improve by an average of 14.68% and 15.71%. Moreover, compared to single-sensor multitarget tracking, the RMSE and MAPE of composite perception fusion results based on the MCGPDAF algorithm are further enhanced by 26.43% and 27.15% on average, which reflects the practicality of the tracking method showcased in this research.

INDEX TERMS Intelligent vehicle, multiconstraint, GPDA, composite perception, fusion, multitarget tracking.

I. INTRODUCTION AND MOTIVATION

An intelligent vehicle is a comprehensive system that encompasses several aspects, including environment perception, path planning, decision-making and assisted driving. As a prerequisite for ensuring correct decision-making and planning control of intelligent vehicles, environmental perception directly determines the intelligence level and autonomous driving ability of vehicles [1], [2]. However, intelligent vehicles must typically face complex, dynamic and uncertain

The associate editor coordinating the review of this manuscript and approving it for publication was Dost Muhammad Khan.

driving environments. Accurate perception and tracking of vehicle target states and quantities has thus become a difficult and critical task in terms of intelligent driving. Since the multitarget tracking of intelligent vehicles involves a series of uncertainty problems, such as random changes in the number of targets, measurement outliers and noise interference, missed sensor detection, and sudden changes in the target motion state, the traditional single-sensor multitarget tracking method cannot yield the tracking accuracy of multitargets in the above complex scenes [3], [4]. Therefore, a multitarget tracking method based on multisource information fusion is highly important for accurately evaluating vehicle obstacle dynamics.

Composite perception, that is, multisensor perception fusion technology, can be categorized into three main types based on the architecture: centralized, distributed and hybrid [5]. The centralized fusion system has low information loss and high data fusion accuracy. However, this centralized processing method involving spatial registration, data association, estimation fusion and other operations has high requirements for communication efficiency and processor performance, and real-time data processing is difficult to guarantee [6]. The distributed fusion system can first process the measurements of each sensor separately and then achieve the combined reasoning and information fusion of multisensor data in the fusion centre. Distributed fusion has low channel capacity requirements, strong real-time performance and fault tolerance, and expansion ease [7], [8]. The hybrid fusion system exploits the advantages of both distributed and centralized systems, but its fusion structure is the most complex of the systems, which increases the burden of system communication and computing power [9]. Distributed fusion has gained extensive recognition and application in the field of multitarget tracking because of its low hardware performance requirements and strong practicability.

At present, the multitarget obstacle tracking method for intelligent vehicles relies mainly on distributed multisensor parallel tracking and real-time fusion to achieve effective target trajectory tracking and state monitoring. As the core technology of modern sensor systems, multitarget tracking algorithms and multisensor perception fusion technology have been widely applied in terms of intelligent driving [10], [11]. However, in actual multitarget obstacle perception scenes, there are uncertainties in the target state and measurement, which directly impact the tracking performance of the multitarget tracking algorithm and the fusion accuracy of multisensor information. Based on the analysis of the existing studies, the current challenges faced by the distributed multitarget tracking algorithm can be summarized as follows: (1) Accurate state update and estimation of multitarget that are close to adjacent targets and difficult to distinguish; (2) Suppress the measurement outliers and process noise arising from the unpredictable road environment; and (3) Accurate generation, update and management of multitarget trajectories.

Current multitarget tracking algorithms can be categorized divided into two primary groups: data association algorithms and random finite sets. Data association algorithms combines the state estimation and update for each target by calculating the mutual association probability between each target and different measurements at discrete times to establish a continuous multitarget trajectory. The representative data association algorithms include the Joint Probabilistic Data Association (JPDA) algorithm, Nearest Neighbour (GNN) algorithm and multiple hypothesis tracking (MHT) algorithm [12]. On the other hand, the multitarget tracking algorithm based on random finite set is a Bayesian filter that utilizes finite set statistics to estimate the state and quantity of multiple targets, without considering data association. Typical multitarget tracking algorithms based on random finite sets include probability hypothesis density (PHD) filters and multi-Bernoulli (MeMBer) filters [13]. However, when handling dense dynamic clutter and unknown prior parameters, the accuracy and performance of the above multitarget tracking algorithm for state estimation and tracking of adjacent targets are still not ideal. Therefore, constructing a robust and efficient vehicle multitarget tracking method in complex time-varying environments is still a topic of great difficulty and research value.

To solve the challenge of multitarget tracking in intelligent vehicles with measurement outliers and time-varying motion states of targets in dense dynamic clutter environments, a Multiconstrained Generalized Probabilistic Data Association Filtering (MCGPDAF) algorithm is proposed. The algorithm utilizes the position and heading data of dynamic targets to construct constraint parameters to calculate the association probabilities between effective measurement combinations and the target trajectories, enabling the robust association of single-sensor multitarget measurements and accurate estimation and tracking of target states under complex working conditions and environments. On this basis, a multitarget obstacle tracking and monitoring method based on composite perception fusion is further constructed. The correlation sequential track association algorithm and covariance cross fusion algorithm are used to conduct track association and the estimation and fusion of target states among multiple sensors, which further improves the tracking accuracy of the multitarget state of the vehicle. In general, the significant contributions of this research are the following aspects: (1) A MCGPDAF algorithm is proposed. (2) The MCGPDAF algorithm solves the problem of single-sensor multitarget tracking under multitarget track crossover or large manoeuvring. It can effectively suppress the errors of measurement associations and motion estimation models and can enhance the accuracy and robustness of vehicle during multitarget tracking. (3) The multitarget tracking of intelligent vehicles in diverse cluttered environments during real driving scenarios is realized, and excellent tracking performance is achieved. Moreover, the tracking accuracy is further improved by multi-sensor fusion.

The main structure of this paper is as follows: This section introduces the research motivation and contribution. Section II discusses existing related research and their shortcomings. Section III expounds on the multi-sensor data preprocessing, spatial registration methods, and the basic principles and formula derivation of MCGPDAF algorithm and composite perception fusion method. Section IV mainly covers the simulation and real vehicle experiment methods and results for multitarget tracking in various environments, analyzing the advantages of the proposed algorithm and fusion architecture. Section V presents the conclusion, providing a comprehensive summary of the primary contents and significant results of this study.

II. RELATED WORK

The tracking and monitoring methods for multitarget obstacles in intelligent vehicles must encompass two factors: a single-sensor multitarget tracking algorithm and a multisensor fusion criterion. Different combinations of multitarget tracking algorithms and fusion criteria will have different effects on the performance of distributed multisensor multitarget tracking.

The single-sensor multitarget tracking algorithms can be categorized into data association algorithms and random finite sets. The GNN and MHT are classical multitarget data association algorithms [14], [15]. However, GNN requires the number of targets as a known prior parameter, and the tracking performance of MHT is severely limited in complex environments such those with as dense targets and low signal-to-noise ratios. To solve these problems, the JPDA algorithm was proposed for multitarget tracking under a dense clutter condition [16]. However, the computational complexity of JPDA is not ideal, which makes it difficult in meeting real-time requirements. To overcome this limitation, lightweight improved algorithms such as the Suboptimal Joint Probabilistic Data Association (SJPDA), Near-optimal Joint Probabilistic Data Association (NJPDA) and Maximum Likelihood Probabilistic Data Association (ML-PDA) have also been proposed successively, but the accuracies of these algorithms has been sacrificed to reduce their complexity [17], [18], [19]. The generalized probabilistic data association (GPDA) algorithm defines new feasibility rules and a method for calculating the interdependent association probability, which greatly reduces the computational complexity and has high computational efficiency and scalability [20], [21]. In addition, The Joint Integrated Probabilistic Data Association (JIPDA) algorithm generates all possible combinations of track-measurement assignments to form joint events, and subsequently computes the posterior probability for each joint event. Based on these probabilities, the data association coefficient for each track is calculated to update the track estimate. The JIPDA algorithm addresses track management when there is an unspecified quantity of targets and a time-varying state, suppresses unnecessary computational power consumption [22].

The application of random finite set theory has produced a new solution to the multitarget tracking problem. Mahler et al. proposed a multisensor multitarget Bayesian filter for multitarget state estimation based on finite set statistics. This method cannot be applied in engineering settings due to the complex integral operation of random finite sets in Bayesian recursion. To solve this problem, Yu [23] successively proposed the PHD and the cardinalized probability hypothesis density (CPHD) filter, which have relatively stable filtering accuracies and high engineering application values. Garcia-Fernandez and Svensson [24] proposed a trajectory probability hypothesis density (TPHD) filter and trajectory cardinalized probability hypothesis density (TCPHD) based on minimized KL divergence, which can infer and update the survival trajectory by recursively propagating Poisson multitrajectory density. In addition, Cao and Zhao [25] proposed a multi-Bernoulli (MeMBer) filter, which can use the multi-Bernoulli distribution to approximate the multitarget posterior density and estimate the target state and number at the current time. However, the above algorithms cannot allocate the track to the target. To solve this problem, Guo et al. [26] proposed a generalized labelled multi-Bernoulli (GLMB) filter to output the target track information. On this basis, Cheng et al. [27] further proposed the Fast Labelled Multi-Bernoulli (FLMB) filter, which achieves the state estimation performance of MeMBer filters and improves the efficiency of target track label estimation. Cai et al. [28], [29] developed a life estimation approach for complex time-varying engineering systems using dynamic Bayesian networks, yielding accurate prediction results and meeting the expected technical performance.

The multisensor fusion criterion plays a crucial role in achieving more accurate target state information by effectively combining the track information from different sensors.Several approaches have been proposed, including convex combination fusion [30], covariance intersection (CI) fusion [31], generalized covariance intersection (GCI) fusion [32] and arithmetic average (AA) fusion [33], [34]. The convex combination fusion algorithm is considered the optimal method for estimation fusion when the local estimation errors of the sensor are not correlated. However, due to the correlation among the local estimations of each sensors during the fusion process, the CI fusion algorithm has been proposed for solving the optimal weighted distributed fusion estimation problem under the condition that the cross-covariance is unknown. Furthermore, to satisfy the fusion of any probability density, the GCI fusion algorithm was proposed. The AA algorithm and the GCI algorithm are both average consensus fusion methods. The GCI algorithm can better suppress false alarms than other algorithms, and the AA algorithm has stronger robustness. In general, the multitarget tracking algorithms for data association classes are suitable for convex combination fusion and CI fusion criteria, and the multitarget tracking algorithms for random finite set classes are suitable for AA fusion and GCI fusion criteria.

In summary, research on distributed multisensor multitarget tracking has made some progress and has been widely used. However, problems such as the precise tracking of adjacent or cross targets, measurement association anomalies, motion estimation model errors, and target track management have not been considered. To solve the above problems, a dynamic multitarget obstacle tracking and monitoring method for vehicle routing based on multiple constraint composite perception association filtering is proposed. This method addresses the problems of vehicle multitarget tracking with target measurement outliers and a time-varying motion state in a dense dynamic clutter environment, improving the tracking performance and monitoring accuracy of multitargets under complex working conditions.

III. TRACKING AND MONITORING OF DYNAMIC MULTITARGET OBSTACLES ON VEHICLE PATHS

Multitarget obstacle tracking is essentially estimating, fusing and continuously monitoring the number and state of targets by utilizing noisy measurement acquired from multiple sensors. Considering the different sensing accuracies and expression characteristics of different sensors, preprocessing and spatial registration are first performed on multisensor data. Furthermore, a MCGPDAF algorithm is proposed, which uses the position and heading information of the dynamic target to construct constraint parameters and enables the robust association of single-sensor multitarget measurements and accurate tracking of the state under complex conditions such as target intersections. On this basis, a multitarget obstacle tracking and monitoring method based on composite perception fusion is further constructed, combining the correlation sequential track association algorithm and the covariance cross fusion algorithm to achieve multisensor multitarget track association and state estimation fusion. To provide a visual representation, the application scenario diagram of the algorithm is indicated in Fig. 1, while the overall architecture of the multitarget obstacle tracking and monitoring method is indicated in Fig. 2.

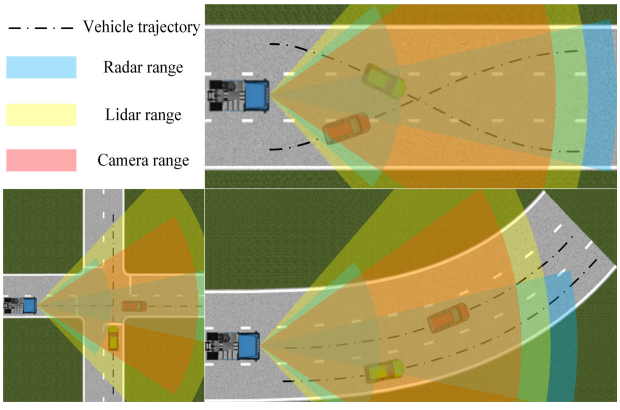

FIGURE 1. The application scenario diagram of the algorithm.

A. MULTISENSOR DATA PREPROCESSING

The ARS408-21SC3 77 GHz millimetre-wave (MMW) radar (Continental AG), Mobileye EyeQ4 smart camera and R-Fans32 lidar (Surestar, Inc.) are used as the perception layers of the distributed fusion system. Considering the different perception characteristics and data expression forms of different sensors, it is necessary to preprocess the MMW radar, lidar and camera data to minimize the influences of dense clutter and invalid targets on the tracking and fusion effects. The perception range and visual field of all the sensors on intelligent vehicle are shown in Fig. 3. The target information of each sensor after data preprocessing during multitarget tracking in the same scene is shown in Fig. 4. This provides more intuitive multitarget brief information for the target tracking algorithm.

Based on the target characteristics obtained by MMW radar, radar targets can be divided into three main categories: (1) nondangerous targets: pedestrians and vehicles far away from the vehicle or outside the motor vehicle lane; (2) false alarm targets: false targets generated by radar measurement noise; and (3) effective goals: real targets other than the above targets. By constraining the horizontal and longitudinal detection ranges of the radar, the interference of nonhazardous targets and some false alarm targets can be mitigated, thereby reducing the calculation time and calculation amount of the multitarget tracking. Considering the detection range needed for safe driving of the vehicle, the longitudinal detection distance and angle range of the radar long-range and short-range are restricted to within 150 m, $\pm 10°$ and 45 m, $\pm 45°$, respectively.

The original lidar signal consists of three-dimensional laser point cloud data, which are characterized by an uneven distribution of pixels and a disordered arrangement of point clouds. Therefore, preprocessing the original point cloud data is essential to attain the position and state of the targets after clustering. Firstly, voxel grid filtering and radius filtering are utilized to process the point cloud data, which can effectively diminish the amount of point clouds and outliers while preserving the shape attributes of the point clouds. Next, the plane grid approach is applied to partition and eliminate ground point cloud data. Thirdly, the approach of region growing is employed to effectively partition the point cloud of the target. Finally, the DBSCAN method is employed for clustering the segmented point clouds of the targets. This method can cluster point clouds of any shape and can effectively address outliers.

The Mobileye EyeQ4 smart camera is used to obtain and process image data. By accurately mapping the pixel position to the actual position, we establish the geometric model of the camera imaging and calculate both the internal and external parameters of the camera, thus achieving the geometric calibration of the camera. The calibrated camera can directly output data such as the category, speed and distance of the targets. Therefore, the camera data are directly preprocessed by using the ID number to filter and eliminate

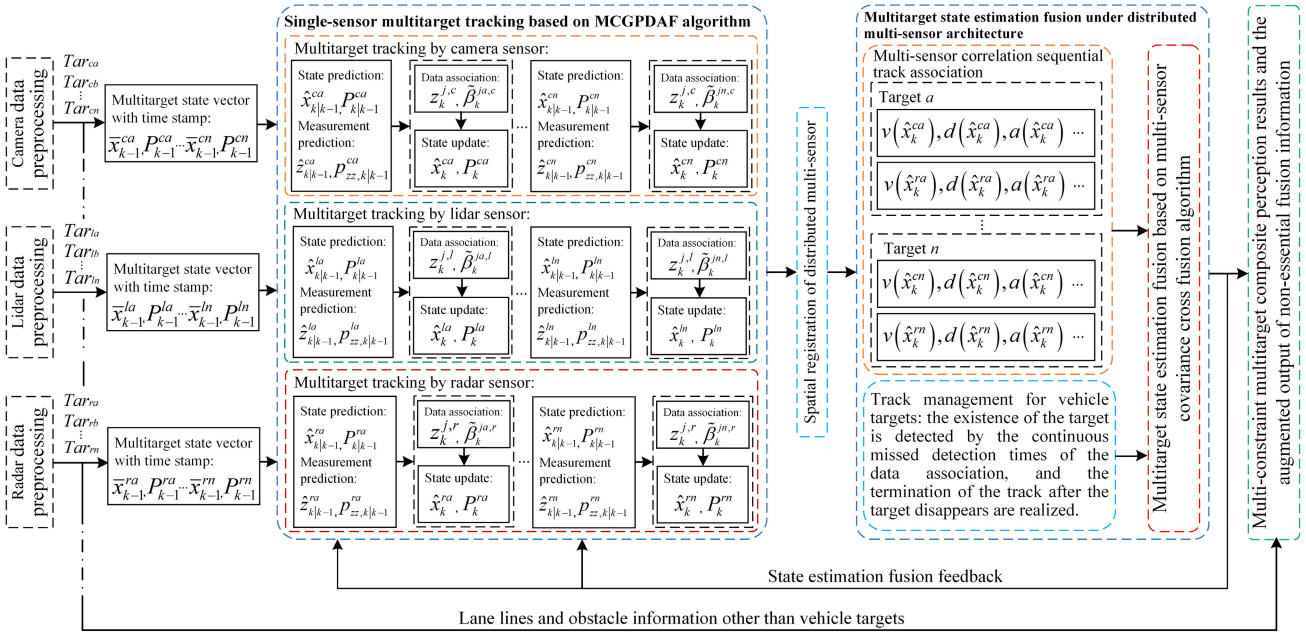

FIGURE 2. The overall architecture of the multitarget obstacle tracking and monitoring method.

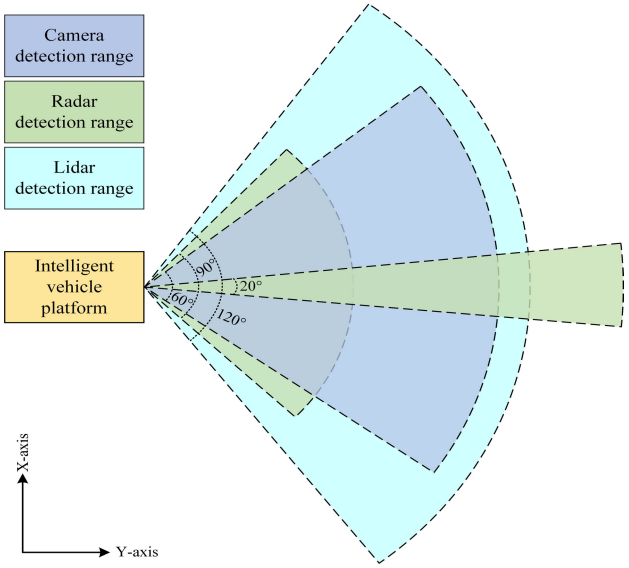

FIGURE 3. The perception range and visual field of all the sensors.

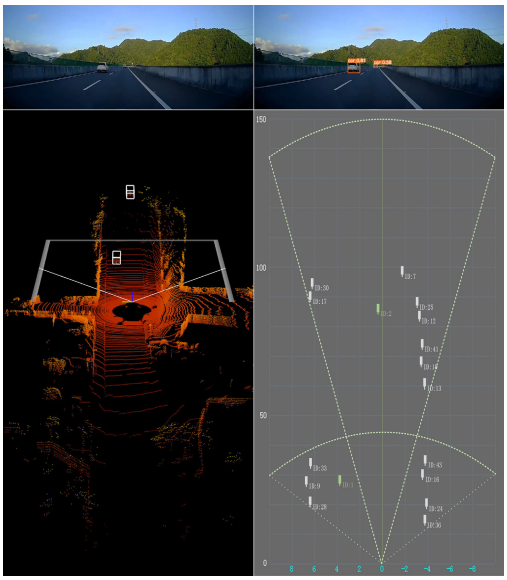

FIGURE 4. Target information of each sensor after data preprocessing in the same scene.

nonessential targets and their associated information outside the motor vehicle lane.

B. SPATIAL REGISTRATION OF DISTRIBUTED MULTISENSOR SYSTEMS

Each sensor on the intelligent vehicle is rigidly connected to the body, and the relative attitude and displacement between each sensor and the vehicle are fixed. Therefore, the data points obtained by each sensor have a unique position coordinate corresponding to the sensor in the environmental coordinate system. In this section, by extracting the corresponding feature points between the image coordinate system and each sensor, and the transformation and unified relationship between the camera coordinates, MMW radar coordinates, lidar coordinates and image pixel coordinates are constructed to enable the spatial registration of multiple sensors.

Separate calibrations are conducted for different sensors so that the normal vectors of the camera, Lidar and MMW radar are parallel to the advancement direction of the vehicle. The camera and image pixel coordinate system are defined as $O_p - x_p y_p$ and $O_c - x_c y_c z_c$, respectively. The z_c axis coincides with the camera optical axis, while the x_c and y_c axis are parallel to the x_p and y_p axis, respectively. On this basis, the projection coordinate systems of the MMW radar, lidar and

camera are established as $O_{rw} - x_{rw}y_{rw}z_{rw}$, $O_{lw} - x_{lw}y_{lw}z_{lw}$ and $O_{cw} - x_{cw}y_{cw}z_{cw}$, respectively. O_{rw}, O_{lw} and O_{cw} are the projection points of each sensor centre above the ground. The x-axis and y-axis of each coordinate system indicates towards the right side and the forward direction of the vehicle body, respectively, while the z-axis is vertical. The projection coordinate systems of the three sensors are positioned parallel to one another in space. The diagram illustrating the spatial relative relationship is depicted in Fig. 5.

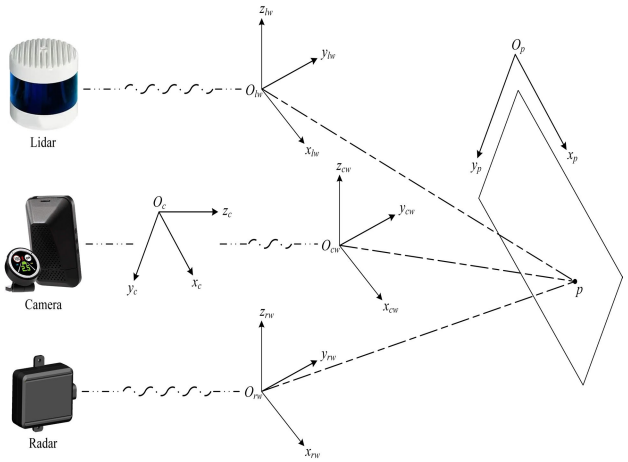

FIGURE 5. The relative relationships of the projection coordinate systems of the three kinds of sensors in space.

According to the pinhole imaging model, the following relationships exist between the $O_p - x_py_p$ and $O_c - x_cy_cz_c$ coordinate system:

$$\begin{cases} \dfrac{x_c}{z_c} = \dfrac{x_p - c_x}{f_x} \\ \dfrac{y_c}{z_c} = \dfrac{y_p - c_y}{f_y} \end{cases} \tag{1}$$

where c_x and c_y are the optical axis offsets.

Through the rotation and translation of the coordinate system, we can obtained the transformation relationship between the $O_c - x_cy_cz_c$ and $O_{cw} - x_{cw}y_{cw}z_{cw}$ coordinate system:

$$\begin{bmatrix} x_c \\ y_c \\ z_c \end{bmatrix} = \begin{bmatrix} 1 & 0 & 0 \\ 0 & -\sin\theta & -\cos\theta \\ 0 & \cos\theta & \sin\theta \end{bmatrix} \begin{bmatrix} x_{cw} \\ y_{cw} \\ z_{cw} \end{bmatrix} + \begin{bmatrix} 0 \\ H\cos\theta \\ H\sin\theta \end{bmatrix} \tag{2}$$

During the tracking of vehicle target, the pavement is generally considered to be a plane, so the z-axis height can be ignored. According to Eq. (1) and Eq. (2), we can obtained the transformation relationship between the $O_p - x_py_p$ and $O_{cw} - x_{cw}y_{cw}z_{cw}$ coordinate system:

$$\begin{cases} x_p = \dfrac{f_x x_{cw} + c_x\,(y_{cw}\cos\theta + H\sin\theta)}{y_{cw}\cos\theta + H\sin\theta} \\ y_p = \dfrac{f_y\,(H\cos\theta - y_{cw}\sin\theta) + c_y\,(y_{cw}\cos\theta - \sin\theta)}{y_{cw}\cos\theta - \sin\theta} \end{cases} \tag{3}$$

The mutual conversion between the $O_{cw} - x_{cw}y_{cw}z_{cw}$ and $O_{rw} - x_{rw}y_{rw}z_{rw}$ coordinate system is achieved by converting the coordinate system:

$$\begin{cases} x_{cw} = x_{rw} - L_x \\ y_{cw} = y_{rw} - L_y \end{cases} \tag{4}$$

According to Eqs. (1), (3) and (4), we can acquired the computational relationship of converting any point in the $O_{rw} - x_{rw}y_{rw}z_{rw}$ to the $O_p - x_py_p$ coordinate system:

$$\begin{cases} x_p = c_x + \dfrac{(x_{rw} - L_x)f_x}{H\sin\theta + (y_{rw} + L_y)\cos\theta} \\ y_p = c_y + \dfrac{[H\cos\theta - (y_{rw} + L_y)\sin\theta]f_y}{H\sin\theta + (y_{rw} + L_y)\cos\theta} \end{cases} \tag{5}$$

where f_x and f_y represent the focal lengths, which are internal parameters of the camera. L_x and L_y are the distances from the x-axis and y-axis in the $O_{rw} - x_{rw}y_{rw}z_{rw}$ coordinate system to the x-axis and y-axis in the $O_{cw} - x_{cw}y_{cw}z_{cw}$ coordinate system, respectively.

Finally, the transformation relationship between the $O_{lw} - x_{lw}y_{lw}z_{lw}$ and $O_p - x_py_p$ coordinate system is attained by using multiple sets of corresponding points:

$$\begin{pmatrix} x_p \\ y_p \\ 1 \end{pmatrix} = K \begin{bmatrix} R & T \\ 0 & 1 \end{bmatrix} \begin{pmatrix} x_{lw} \\ y_{lw} \\ z_{lw} \\ 1 \end{pmatrix} \tag{6}$$

The above coordinate transformation is used to solve $(R \mid T)$, and the translation vector T and the rotation matrix R can be calculated given at least four groups of corresponding points. K is the internal parameter matrix of the camera.

C. MULTITARGET TRACKING AND STATE ESTIMATION

1) GENERALIZED PROBABILITY DATA ASSOCIATION

The Generalized Probabilistic Data Association (GPDA) algorithm defines new feasibility rules using generalized joint events. When the count of targets is T and the count of measurements is m_k, the new feasibility rules are as follows:

(1) Each measurement can come from one or more targets;

(2) Each target can have one or more measurements;

(3) The probability of one-to-one correspondence between any measurement and the target is not less than the probability of associated events in rules (1) and (2).

According to the definition rules, the set of generalized joint events is segregated into two subsets. The generalized events satisfying feasibility rule (1) take the target as the basis, and the generalized events satisfying feasibility rule (2) take the measurement as the basis.

Given the associated event θ_{jt}, the state variable of target t is assumed to follow a normal distribution with mean $\hat{x}_t(k \mid k-1)$ and variance $P_t(k \mid k-1)$. The probability density function f_{jt} between the target measurement and each individual target is subsequently computed.

The probability density function f_{jt} is calculated as follows:

$$f_{jt} = p\left(z_{jt} \mid m_k, Z_t^k\right) = \begin{cases} P_g^{-1}\left|2\pi S_t^f(k)\right|^{-\frac{1}{2}} \\ \quad \exp\left[-\frac{1}{2}\left[v_{jt}^f(k)\right]^T\left[S_t^f(k)\right]^{-1}v_{jt}^f(k)\right] \\ \quad j \neq 0, t \neq 0 \\ (nV)^{-1}\left(1 - P_d P_g\right) \quad j = 0, t \neq 0 \\ \lambda \quad j \neq 0, t = 0 \\ 0 \quad j = 0, t = 0 \end{cases} \tag{7}$$

$$v_{jt}^f(k) = z_{jt}(k) - \hat{Z}_t(k \mid k-1) \tag{8}$$

where $S_t^f(k)$ denotes the residual covariance matrix of target t, $\hat{Z}_t(k \mid k-1)$ denotes the one-step prediction of the measurement of target t at time k, $z_{jt}(k)$ is the j-th measurement of target t at time k.$v_{jt}^f(k)$ and $S_t^f(k)$ denote the innovation and innovation covariance matrix of target t, respectively. P_d is the probability of target detection, P_g is the probability of measurement within the correlation gate, and λ represents the clutter density, which refers to the number of false measurements per unit space.

The probability density function $f_{0t}(j = 0, t \neq 0)$ represents the scenario in which the target has not obtained any valid measurements; $f_{j0}(j \neq 0, t = 0)$ indicates that a measurement does not pertain to any of the system targets; $f_{00}(j = 0, t = 0)$ indicates that the zero target is associated with the zero measurement, which is of no practical significance.

The probability statistical matrix N is generated based on the statistical distance between the measurement j and the target t.

$$N = \left[f_{jt}\right] \tag{9}$$

2) MULTICONSTRAINED GENERALIZED PROBABILISTIC DATA ASSOCIATION FILTERING ALGORITHM

During the process of multitarget tracking, the intricate variations in the real environment and target motion can result in an escalation of measurement outliers and process noise. The presence of unknown environmental clutter prior information and limited target motion models often prove inadequate in effectively addressing this issue, thereby significantly impacting the performance and accuracy of multitarget tracking. The present study addresses this concern by proposing a novel algorithm, namely the MCGPDAF algorithm.

In accordance with the laws of motion governing vehicle targets, changes in their motion states such as speed, direction and acceleration are continuous processes. From the perspective of sensors like radar or cameras, these continuous changes are most intuitively and accurately reflected in the variations of target position and heading angle. Therefore, during multitarget tracking, there should be no sudden shifts observed between adjacent moments in terms of target position and heading angle values. This provides a theoretical foundation for distinguishing effective measurements from irrelevant ones under dense clutter conditions. Furthermore, in the case of target crossing, obvious differences and distinctions in positions and heading angles can be observed among different targets, and both of which exhibit sustainable estimation characteristics. Consequently, incorporating target position and heading angle as constraint parameters can mitigate measurement-track association uncertainty and effectively enhance multitarget tracking performance of intelligent vehicles operating under complex environments.

The MCGPDAF algorithm leverages the position and heading information of dynamic targets to establish constraint parameters for computing the innovation of position and heading angles between the predicted points and measurement points of multitarget trajectory. It assigns higher correlation weights to measurements with smaller innovations, thereby mitigating the adverse effects of process noise and measurement outliers on the interconnection between the targets and the measurements. This algorithm achieves robust association and accurate tracking of multiple target measurements in scenarios involving close proximity or intersection of targets. Additionally, a fading factor is incorporated in the filtering process to adaptively adjust the time-varying gain matrix, thereby enabling real-time computation of residuals for multitarget state estimation. This ensures the residual sequence remains orthogonal and further mitigates the impact of measurement anomalies and process noise, ultimately enhancing the accuracy of multitarget tracking and state estimation. Finally, by constructing a target existence inspection rule to determine the generation or termination of each target track, the maintenance and management of multitarget tracks are realized, and the efficiency of multitarget data association is further improved. The process of the MCGPDAF is revealed in Algorithm 1.

Problem Description:

During vehicle multitarget tracking, the state equation and measurement equation of target t are expressed as follows:

$$x^t(k) = F^t(k-1)x^t(k-1) + v^t(k-1) \quad t = 1, 2, \ldots T \tag{10}$$

$$z_j(k) = H(k)x^t(k) + w^t(k) \quad t = 1, 2, \ldots T; j = 1, 2, \ldots m_k \tag{11}$$

where T represents the overall count of targets and m_k is the effective measurement generated by the sensor. $x^t(k)$ refers to the state vector of target t at time k, $z_j(k)$ denotes the j-th measurement vector of the sensor at time k. Furthermore, $H(k)$ and $F^t(k-1)$ denote the measurement matrix and the state transition matrix, respectively. The process noise $v^t(k-1) \sim N\left(0, Q^t(k-1)\right)$ and the measurement noise $w^t(k) \sim N\left(0, R^t(k)\right)$ are independent zero-mean Gaussian white noises.

The effective measurement set of the sensor at time K is:

$$Z(k) = \left\{z_1(k), z_2(k), \ldots, z_{m_k}(k)\right\} \tag{12}$$

The set of effective measurement acquired by the sensor from the initial time until time k is represented as Z^k, where the effective measurement set belonging to target t is represented by Z_t^k.

$$Z^k = \{Z(1), Z(2), \ldots, Z(k)\} \tag{13}$$

Assuming that each measurement incorporates information regarding the position and heading of the target, then:

$$z_j(k) = \left\{z_j^{\zeta}(k), z_j^{\gamma}(k)\right\} \tag{14}$$

The probability density function between measurement j and target t can be expressed as:

$$p\left(z_j^{\zeta}(k), z_j^{\gamma}(k) \mid Z^k\right) = p\left(z_j^{\zeta}(k) \mid Z^{k,\zeta}\right) \cdot p\left(z_j^{\gamma}(k) \mid Z^{k,\gamma}\right) \tag{15}$$

where $Z^{k,\zeta}$ and $Z^{k,\gamma}$ respectively denote the cumulative sets of target position and heading angle measurements up to time k.

Step 1: Initialize the mean and variance of the target state $\hat{x}^t(0 \mid 0)$ and $P^t(0 \mid 0)$ and predict each target state and its covariance.

$$\hat{x}^t(k \mid k-1) = F^t(k-1)\hat{x}^t(k-1 \mid k-1) \tag{16}$$

$$P^t(k \mid k-1) = F^t(k-1)P^t(k-1 \mid k-1) \times \left[F^t(k-1)\right]^T + Q^t(k-1) \tag{17}$$

Step 2: Determine the effective measurement of each target.

When $r_m^t(k)^2 \leq r_G^2$, the measurements are considered valid.

$$r_m^t(k)^2 = \left[Z_t^k - H(k)\tilde{x}^t(k \mid k-1)\right] S^t(k)^{-1} \times \left[Z_t^k - H(k)\tilde{x}^t(k \mid k-1)\right]^T \leq r_G^2 \tag{18}$$

Step 3: Calculate the probability density function under different constraints.

By calculating the variation of the position $\Delta d_j^t(k)$ between the predicted trajectory point of the target and each measurement point at time k, we obtain the innovation $v_{jt}^{\zeta}(k)$ regarding the position of the target.

$$\Delta d_j^t(k) = v_{jt}^{\zeta}(k) = z_{jt}^{\zeta}(k) - \hat{Z}_t(k \mid k-1) \tag{19}$$

where $z_{jt}^{\zeta}(k)$ denotes the j-th position measurement of target t at time k, while $\hat{Z}_t(k \mid k-1)$ represents the one-step prediction of the measurement of target t at time k.

According to the definition of geometric spatial distance, a smaller positional deviation between the predicted point of a target trajectory and measurement point at the same moment indicates a reduced geometric spatial distance. This implies an increased probability that the measurement belongs to the target trajectory.

Therefore, appropriate position weights are assigned to each measurement point based on the magnitude of $\Delta d_j^t(k)$, and the probability density function ζ_{jt} between the positional measurement and the corresponding target is computed.

$$\zeta_{jt} = p\left(z_j^{\zeta}(k) \mid m_k, Z_t^k\right) \tag{20}$$

The variation of the heading angle $\Delta\delta_j^t(k)$ between the predicted point of the target trajectory and each measurement point should be calculated simultaneously within the same observation dimension of the sensor.

The heading angle $\delta^t(k)$ of the predicted point of the target trajectory at time k is defined based on the direction of the vector $\hat{x}^t(k-1)\hat{x}^t(k \mid k-1)$, and the calculation for $\delta^t(k)$ can be expressed as follows, (21), as shown at the bottom of the next page.

The heading angle $\tilde{\delta}_j^t(k)$ of each measurement point at time k is defined based on the direction of the vector $\hat{x}^t(k-1)z_j(k)$, and the calculation for $\tilde{\delta}_j^t(k)$ can be expressed as follows:

$$\tilde{\delta}_j^t(k) = \pi\,(1 - e_m) + e_m \frac{\arccos\left(x_j'(k) - \hat{x}^{t'}(k-1)\right)}{\sqrt{\left(x_j'(k) - \hat{x}^{t'}(k-1)\right)^2 + \left(y_j'(k) - \hat{y}^{t'}(k-1)\right)^2}} \tag{22}$$

where $\hat{x}^t(k-1)$ denotes the state estimation of target t at time $k-1$, $\hat{x}^{t'}(k-1)$ and $\hat{y}^{t'}(k-1)$ are the components of $\hat{x}^t(k-1)$, $\hat{x}^t(k \mid k-1)$ represents the state prediction value of target t at time k, $\hat{x}^{t'}(k \mid k-1)$ and $\hat{y}^{t'}(k \mid k-1)$ are the components of $\hat{x}^t(k \mid k-1)$, $z_j(k)$ denotes the j-th measurement of the sensor at time k; $x_j'(k)$ and $y_j'(k)$ are the components of $z_j(k)$, e_c and e_m determine the vector directions of vectors $\hat{x}^t(k-1)\hat{x}^t(k \mid k-1)$ and $\hat{x}^t(k-1)z_j(k)$, respectively.

$$e_c = \frac{\left(\hat{y}^{t'}(k \mid k-1) - \hat{y}^{t'}(k-1)\right)}{\left|\hat{y}^{t'}(k \mid k-1) - \hat{y}^{t'}(k-1)\right|} \tag{23}$$

$$e_m = \frac{\left(y_j(k) - \hat{y}^{t'}(k-1)\right)}{\left|y_j(k) - \hat{y}^{t'}(k-1)\right|} \tag{24}$$

By calculating the variation of the heading angle $\Delta\delta_j^t(k)$ between the predicted trajectory point of the target and each measurement point at time k, we obtain the innovation $v_{jt}^{\gamma}(k)$ regarding the heading angle of the target.

$$\Delta\delta_j^t(k) = v_{jt}^{\gamma}(k) = \tilde{\delta}_j^t(k) - \delta^t(k) \tag{25}$$

Based on the motion characteristics of vehicles, the variation in the motion state of the target between adjacent moments is continuous and devoid of abrupt changes. Consequently, a smaller $\Delta\delta_j^t(k)$ value signifies a higher probability of correlation between the measurement and the target trajectory. Appropriate directional weights are assigned

to each measurement point based on the magnitude of $\Delta\delta_j^t(k)$, and the probability density function γ_{jt} between the measurement of the heading angle and the corresponding target is computed.

$$\gamma_{jt} = p\left(z_j^{\gamma}(k) \mid m_k, Z_t^k\right) \tag{26}$$

Step 4: Calculate the interconnection probability.

According to Eq. (13), the constraints on target position and heading are introduced into the data association event θ_{jt}. Subsequently, the probability density function $p_{jt}(j \neq 0, t \neq 0)$ of the data association event θ_{jt} is computed, that is, the statistical distance between measurement $j(j \neq 0)$ and target $t(t \neq 0)$. The calculation can be formulated as follows:

$$\begin{aligned} p_{jt} &= \zeta_{jt} \cdot \gamma_{jt} = p\left(z_j^{\zeta}(k) \mid m_k, Z_t^k\right) \cdot p\left(z_j^{\gamma}(k) \mid m_k, Z_t^k\right) \\ &= P_g^{-1} \left|2\pi S_t^{\zeta}(k)\right|^{-\frac{1}{2}} \exp\left[-\frac{1}{2}\left[v_{jt}^{\zeta}(k)\right]^T \left[S_t^{\zeta}(k)\right]^{-1} v_{jt}^{\zeta}(k)\right] \\ &\quad \cdot \left|2\pi S_t^{\gamma}(k)\right|^{-\frac{1}{2}} \exp\left[-\frac{1}{2}\left[v_{jt}^{\gamma}(k)\right]^T \left[S_t^{\gamma}(k)\right]^{-1} v_{jt}^{\gamma}(k)\right] \end{aligned} \tag{27}$$

where $v_{jt}^{\zeta}(k)$ and $v_{jt}^{\gamma}(k)$ represent the innovations of the target's position and heading angle, $S_t^{\zeta}(k)$ and $S_t^{\gamma}(k)$ denote the innovation covariance matrices of the target's position and heading angle, respectively, P_g represents the probability of a measurement falling within the association gate. The calculation of probability density functions $p_{0t}(j = 0, t \neq 0)$, $p_{j0}(j \neq 0, t = 0)$ and $p_{00}(j = 0, t = 0)$ can be referred to as Eq. (7).

To eradicate the influences of varying gauges on the weighting results, the p_{jt} is normalized based on the target and measurement, respectively, and the probability statistical matrices P_{jt} and P'_{jt} are generated:

$$P_{jt} = \frac{p_{jt}}{\sum_{t=0}^{T} p_{jt}} \tag{28}$$

$$P'_{jt} = \frac{p_{jt}}{\sum_{j=0}^{m_k} p_{jt}} \tag{29}$$

Finally, the interconnection probability β_{jt} between measurement j and target t is calculated by applying Bayes' theorem.

$$\tilde{\beta}_{jt}(k) = \frac{1}{c}\left[P_{jt} \prod_{tr=0}^{T} \sum_{r=0}^{m_k} P_{r,tr} + P'_{jt} \prod_{r=0}^{m_k} \sum_{tr=0}^{T} P'_{r,tr}\right] \tag{30}$$

where r and tr represent the corresponding measurement labels and target labels, respectively, and c is the normalization coefficient.

Step 5: Combination estimation and state updating.

Firstly, the fading factor $\eta(k)$ is introduced into the estimation process to obtain an appropriate time-varying gain matrix, ensuring that the residual sequence remains orthogonal throughout.

$$\eta(k) = \begin{cases} \eta_0, & \eta_0 > 1 \\ 1, & \eta_0 \leq 1 \end{cases} \tag{31}$$

The calculation of η_0 can be expressed as follows:

$$\eta_0 = \frac{\mathrm{tr}\left[V_{0,k} - R_k\right]}{\mathrm{tr}\left[P_{y_k} - R_k\right]} \tag{32}$$

where P_{y_k} denotes the error covariance of the measurement vector, R_k denotes the error covariance of the measurement noise, and the specific derivation of η_0 can be found in reference [35].

The iterative calculation expression for the residual covariance matrix $V_{0,k}$ is as follows:

$$V_{0,k} = E\left[v_k v_k^T\right] = \begin{cases} v_k v_k^T & k = 1 \\ \dfrac{\mu V_{0,k-1} + v_k v_k^T}{1+\rho} & k > 1 \end{cases} \tag{33}$$

The combined estimation of all hypotheses is obtained:

$$\hat{x}_j^t(k \mid k) = \tilde{x}^t(k \mid k-1) + K^t(k)\left[z_j(k) - H(k)\tilde{x}^t(k \mid k-1)\right] \tag{34}$$

$$P_j^t(k \mid k) = P^t(k \mid k-1) - \eta(k) \cdot K^t(k) S^t(k)^{-1} \left[K^t(k)\right]^T \tag{35}$$

Eventually, the updated target state and covariance matrix are determined:

$$\hat{x}^t(k \mid k) = \sum_{j=0}^{m_k} \tilde{\beta}_{jt}(k) \hat{x}_j^t(k \mid k) \tag{36}$$

$$\begin{aligned} P^t(k \mid k) = \sum_{j=0}^{m_k} \tilde{\beta}_{jt}(k) \Bigg[P_j^t(k \mid k) + \hat{x}_j^t(k \mid k)\left[\hat{x}_j^t(k \mid k)\right]^T\Bigg] \\ - \hat{x}^t(k \mid k)\left[\hat{x}^t(k \mid k)\right]^T \end{aligned} \tag{37}$$

Step 6: Inspect the target existence. When the target disappears within the range of vehicle perception, the system needs to determine and eliminate the trajectory of the target to avoid occupying nonessential computing and storage resources and affecting the data association efficiency of other targets. The track termination threshold is indicated as ξ_L, the count of consecutive missed detections of the target t measurement-track association is n_L^t, and the initial value is 0. When the track described by target t at a certain time cannot obtain the associative measurement, n_L^t is increased by 1, and the trajectory is maintained by using

$$\delta^t(k) = \pi\left(1 - e_c\right) + e_c \frac{\arccos\left(\hat{x}^{t'}(k \mid k-1) - \hat{x}^{t'}(k-1)\right)}{\sqrt{\left(\hat{x}^{t'}(k \mid k-1) - \hat{x}^{t'}(k-1)\right)^2 + \left(\hat{y}^{t'}(k \mid k-1) - \hat{y}^{t'}(k-1)\right)^2}} \tag{21}$$

the measurement prediction value at the current time. If the number of consecutive missed detections is $n_L^t > \xi_L$, the target is determined to disappear, and the target tracking is terminated.

Algorithm 1 Multiconstrainted Generalized Probability Data Association Filtering Algorithm (MCGPDAF)

Iutput: $\{\hat{x}^t(k-1), P^t(k-1)\}, Z(k)$
Initialize $\hat{x}^t(0 \mid 0), P^t(0 \mid 0), r_G^2$
for $t = 1, 2, \ldots T$ and $j = 1, 2, \ldots m_k$ **do**
  Prediction of the state: $\hat{x}^t(k \mid k-1)$ and $P^t(k \mid k-1)$
  while $r_m^t(k)^2 \le r_G^2$ **do**
    Calculate $\Delta d_j^t(k)$ and ζ_{jt} according to Eq. (19) - (20)
    Calculate $\Delta \delta_j^t(k)$ and γ_{jt} according to Eq. (21) - (26)
    Calculate p_{jt} and normalize it according to Eq. (27) - (29)
    Calculate $\tilde{\beta}_{jt}(k)$
  end while
  Calculate the fading factor $\eta(k)$ according to Eq. (31) - (33)
  Combination estimation: $\hat{x}_j^t(k \mid k)$ and $P_j^t(k \mid k)$
  Update $\hat{x}^t(k \mid k)$ and $P^t(k \mid k)$
  Estimate the target existence and manage multiple target tracks
end for
Return $\hat{x}^t(k \mid k), P^t(k \mid k)$
Output: $\hat{x}^t(k \mid k), P^t(k \mid k)$

D. MULTISENSOR CORRELATION SEQUENTIAL TRACK ASSOCIATION

To achieve the optimal matching of the same target among multiple sensors during vehicle multitarget obstacle tracking and monitoring, the correlation sequential association algorithm is used to correlate the estimated tracks of multisensor targets in this paper. The correlation sequential algorithm accounts for the correlation between the historical correlation data and the state estimation errors on the basis of the traditional modified correlation method and can achieve better multitrajectory association performance under complex conditions such as dense clutter and target crossover.

Hypothesis The set of targets tracked by any two sensors c and r is as follows:

$$N_c = \{1, 2, 3, \ldots, T_c\}, N_r = \{1, 2, 3, \ldots, T_r\} \tag{38}$$

The target state estimation difference between two sensors at time k is indicated as follows:

$$D_{ab}^k = \{d_{ab}(i)\} \quad i = 1, 2, 3, \ldots, k; a \in N_c; b \in N_r \tag{39}$$

where $d_{ab}(l) = \hat{x}_a^c(k) - \hat{x}_b^r(k), \hat{x}_a^c(k)$ denotes the state estimation value of sensor c to target a, and $\hat{x}_b^r(k)$ denotes the state estimation value of sensor r to target b.

Let H_0 and H_1 be the following assumptions: H_0 indicates that the state estimations $\hat{x}_a^c(k)$ and $\hat{x}_b^r(k)$ belong to the same target; H_1 indicates that the state estimations $\hat{x}_a^c(k)$ and $\hat{x}_b^r(k)$ do not belong to the same target.

The likelihood function ratios of the joint probability density of H_0 and H_1 are constructed as follows:

$$L(D_{ab}^k) = \frac{f_0(D_{ab}^k \mid H_0)}{f_1(D_{ab}^k \mid H_1)} \tag{40}$$

The logarithmic likelihood function of the above equation is:

$$\ln L(D_{ab}^k) = -\frac{1}{2}\sum_{i=1}^{k}[d_{ab}(k)]^T B_{ab}(k)^{-1} d_{ab}(k) + C \tag{41}$$

where $B_{ab}(k) = P_a^c(k) + P_b^r(k) - P_{ab}^{cr}(k) - P_{ba}^{rc}(k)$ and C is a constant.

According to Eq. (41), the modified log-likelihood function is defined as:

$$\begin{aligned}\rho_{ab}^k &= \sum_{i=1}^{k}[d_{ab}(i)]^T B_{ab}(i)^{-1} d_{ab}(i) \\ &= \rho_{ab}(k-1) + [d_{ab}(k)]^T B_{ab}(k)^{-1} d_{ab}(k)\end{aligned} \tag{42}$$

where ρ_{ab}^k obeys the χ^2 distribution with kn_x degrees of freedom.

Finally, hypotheses H_0 and H_1 are tested. If

$$\rho_{ab}^k \le \delta(k) \tag{43}$$

then H_0 holds; otherwise, H_1 holds. The threshold $\delta(k)$ is chosen according to the distribution of χ^2, and δ satisfies:

$$p\{\rho_{ab}^k > \delta(k) \mid H_0\} = \alpha \tag{44}$$

where α is the significance level of the test, usually 0.05.

E. MULTISENSOR COVARIANCE CROSS FUSION

To achieve the optimal weighted distributed fusion estimation under the condition of unknown crosscovariance, the covariance intersection algorithm is employed to fuse the target state estimation of the multisensor. The covariance intersection algorithm uses local state estimation and its error variance information for fusion and estimation, which avoids complex correlation calculations, and the fusion result has good conservatism and consistency.

The batch covariance Intersection algorithm is used to obtain the multisensor fusion estimate $\hat{x}_{CI}(t)$, and the upper bounds of the actual error variance $P_{CI}, \hat{x}_{CI}(t)$ and P_{CI} can be expressed as follows:

$$\begin{aligned}\hat{x}_{CI}(t) = P_{CI}[&\omega_1 P_1^{-1}\hat{x}_1(t) + \omega_2 P_2^{-1}\hat{x}_2(t) \\ &+ \cdots + \omega_L P_L^{-1}\hat{x}_L(t)]\end{aligned} \tag{45}$$

$$P_{CI} = \left[\omega_1 P_1^{-1} + \omega_2 P_2^{-1} + \cdots + \omega_L P_L^{-1}\right]^{-1} \tag{46}$$

where the optimal parameters are $\omega_i \in [0, 1]$, and $\omega_1 + \omega_2 + \cdots + \omega_L = 1$.

The minimizing performance index $\min_{\omega_i\in(0,1)} \mathrm{tr}\,(P_{CI})$ is:

$$\min_{\omega_i\in(0,1)} \mathrm{tr}\,(P_{CI}) = \min_{\omega_i\in(0,1)} \mathrm{tr}\left\{\left[\omega_1 P_1^{-1} + \omega_2 P_2^{-1} + \cdots + \omega_L P_L^{-1}\right]^{-1}\right\} \quad (47)$$

IV. SIMULATION EXPERIMENT AND RESULT ANALYSIS

A. PARAMETER AND SCENARIO SETTING FOR SIMULATION EXPERIMENT

To assess the superiority of the proposed MCGPDAF algorithm for multitarget tracking, a simulation experiment considering the tracking issue of single sensor multitarget complex manoeuvring in dense dynamic clutter environment is conducted. In this experiment, Prescan8.5, MATLAB2020a and an IPC equipped with a Core i9-12900K are employed as the experiment platform for joint simulation. The simulation scenario encompasses complex manoeuvring conditions such as target crossing, turning and velocity variation. The constant velocity (CV) motion model is employed to estimate the approximate target state to assess the multitarget tracking performance of the algorithm in case of the errors of the motion estimate model. The state vector of the system can be expressed as $x_k = [x_k, \dot{x}_k, y_k, \dot{y}_k]^T$, where x_k and y_k represent the relative longitudinal and transverse distances, while $\dot{x}_k$ and $\dot{y}_k$ represent the relative longitudinal and transverse velocities. The state equation of the system under the CV model is indicated as follows:

$$x_k = F_{CV} \cdot x_{k-1} + \omega_{CV} \quad (48)$$

where F_{CV} represents the status transition matrix, ω_{CV} represents the process noise, and the parameter expressions F_{CV} and ω_{CV} are provided in reference [36].

According to the mapping relation between the target state space and the measurement space within the polar coordinates system, the measurement equation can be indicated as follows:

$$z_k = \begin{bmatrix} r_k \\ \phi_k \\ \tau_k \end{bmatrix} + v_k = \begin{bmatrix} \sqrt{x_k^2 + y_k^2} \\ \arctan\dfrac{y_k}{x_k} \\ \dfrac{x_k\dot{x}_k + y_k\dot{y}_k}{\sqrt{x_k^2 + y_k^2}} \end{bmatrix} + v_k \quad (49)$$

where the measurement vector of the radar sensor includes the centroid position (r_k, φ_k) and the radian velocity τ_k of the moving target and v_k represents the system measurement noise.

To fully validate the virtues of the proposed algorithm in multitarget tracking, a simulation experiment is performed considering multitarget tracking working conditions such as target crossing, turning manoeuvres and speed changes. In the simulation experiment, two target vehicles and a tracking vehicle are established, and the tracking vehicle is equipped with a MMW radar sensor to track multiple targets. The environment clutter density $\lambda = 2 \times 10^{-4}$. The sampling period of the MMW radar is 0.01 s, while the total duration of simulation observation is 45 s. The original state of the target T_1 is $x_0 = [100\ \mathrm{m}, 14.1\ \mathrm{m/s}, 58.5\ \mathrm{m}, 0\ \mathrm{m/s}]^T$. This target is subjected to a uniformly accelerated motion at $0 \sim 23$ s and $33 \sim 45$ s and a uniformly decelerated motion at $23 \sim 33$ s. The original state of the target T_2 is $x_0' = [140\ \mathrm{m}, 16.7\ \mathrm{m/s}, 51.5\ \mathrm{m}, 0\ \mathrm{m/s}]^T$. This target is subjected to a uniformly accelerated motion at $0 \sim 22$ s and $32 \sim 45$ s and a uniformly decelerated motion at $22 \sim 32$ s. The original state of the tracking vehicle T_0 is $x_I = [140\ \mathrm{m}, 13.8\ \mathrm{m/s}, 55\ \mathrm{m}, 0\ \mathrm{m/s}]^T$, and the vehicle is subjected to a uniformly accelerated motion at $0 \sim 24$ s and $37 \sim 45$ s and a uniformly decelerated motion at $24 \sim 37$ s. The simulation scenario and vehicle trajectory are indicated in Fig. 6.

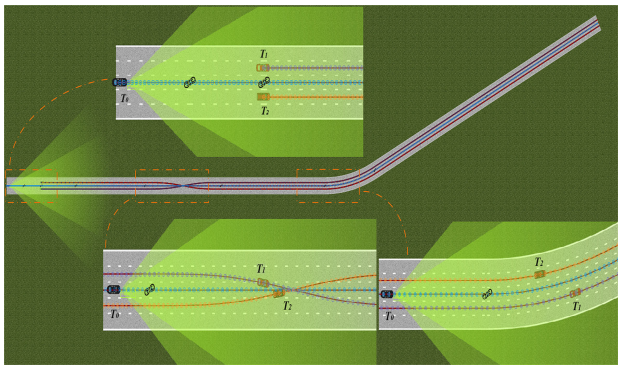

FIGURE 6. The simulation scenario and vehicle trajectory.

B. SIMULATION RESULTS ANALYSIS

In the above simulation scenarios, the JIPDAF [22] and FLMB [27] algorithms are compared with the MCGPDAF algorithm proposed in this research to verify the multitarget tracking performance of the proposed algorithm. Taking the root mean square error (RMSE) and mean absolute percentage error (MAPE) as evaluation indicators of the multitarget tracking accuracy of the algorithm.

$$RMSE = \sqrt{\frac{1}{N}\sum_{i=1}^{N}\left(\hat{x}_i - x_i\right)^2} \quad (50)$$

$$MAPE = \frac{1}{N}\sum_{i=1}^{N}\left|\frac{\hat{x}_i - x_i}{x_i}\right| \times 100\% \quad (51)$$

where $\hat{x}_i$ and x_i represent the optimum estimated value and the truth value of the relative speed or relative distance of each target in the multitarget tracking process, respectively. Moreover, N denotes the total sampling times of the sensor.

Using the above three algorithms to track multitargeted vehicles, the relative velocity and relative distance between the tracking vehicle T_0 and the target T_1 are obtained as indicated in Fig. 7a and 7b, respectively. The relative velocity and relative distance between the tracking vehicle T_0 and the target T_2 are indicated in Fig. 8a and 8b, respectively. The multitarget tracking accuracy results of the different algorithms are revealed in Table 1 and Fig. 9. The multitarget

tracking performances of the algorithms are compared and analysed according to the above simulation results. When the targets T_1 and T_2 perform cross motion and turn manoeuvres, the target measurement and data association are abnormal, resulting in an increased RMSE of the above three algorithms for the relative velocity and relative distance of the tracking target. When compared with the JIPDAF and FLMB algorithms, the MCGPDAF algorithm has the best tracking accuracy and error convergence performance when the target intersects and wide-range manoeuvres. This is because the multiparameter constraint mechanism constructed by the MCGPDAF algorithm gives the algorithm a higher robustness and data association accuracy, enabling it to better restrain the affects of measurement association anomalies and the errors of motion estimation model on the estimation precision in the process of multitarget tracking. Therefore, the MCGPDAF algorithm can achieve higher multitarget tracking accuracy and greater error convergence performance given target crossover and large manoeuvring.

Table 1 and Fig. 9 show that in multitarget tracking, the MCGPDAF algorithm is superior to the other two algorithms regarding the MAPE and RMSE of the relative velocity and relative distance, respectively, and has the highest tracking accuracy. The MCGPDAF algorithm is employed to track the relative velocity and relative distance of the target T_1, and the resulting RMSE values are 0.0824 m/s and 0.1924 m, while the MAPE values are 1.3962% and 1.6837%, respectively. The MCGPDAF algorithm is also employed to track the relative velocity and relative distance of the target T_2, and the resulting RMSE values are 0.0768 m/s and 0.1891 m, while the MAPE values are 1.3125% and 1.6592%, respectively. Compared with the results of the JIPDAF algorithm, when the MCGPDAF algorithm tracks the target T_1, the RMSEs of the relative velocity and the relative distance improve by 28.72% and 30.32%, respectively, and the MAPEs enhance by 29.72% and 31.61%, respectively. When tracking the target T_2, the RMSEs of the relative velocity and the relative distance improve by 29.09% and 29.41%, respectively, and the MAPEs enhance by 29.70% and 29.85%, respectively. Compared with the results of the FLMB algorithm, when the MCGPDAF algorithm tracks target T_1, the RMSEs of the relative velocity and relative distance improve by 17.27% and 19.23%, respectively, and the MAPEs enhance by 17.35% and 19.34%, respectively. The results of tracking target T_2 show that the RMSEs of the relative velocity and relative distance improve by 19.33% and 18.42%, respectively, and the MAPEs enhance by 19.27% and 17.92%, respectively. In summary, the experiments and analysis show that the MCGPDAF algorithm has excellent multitarget tracking performance and accuracy and has great advantages over the JIPDAF algorithm and the FLMB algorithm.

V. EXPERIMENT AND ANALYSIS OF REAL VEHICLE

To validate the multitarget tracking performance and application effect of the proposed dynamic multitarget obstacle tracking and monitoring method in real scenes, real vehicle experiments are conducted. The construction of the experimental platform is founded on the overall architecture of the multitarget obstacle tracking and monitoring method in Fig. 2. According to the experimental results, the multitarget tracking performances before and after perception fusion are compared and analysed, and conclusions are drawn.

A. INTEGRATION OF THE EXPERIMENTAL PLATFORM

The experimental platform for real-world vehicle experimental comprises two primary components: the hardware system and the software platform. The hardware system was composed of an industrial computer (Model ARK3500L, Core i9, Advantech, Inc., Suzhou, China), a MMW radar (Model ARS408-21SC3, 77 GHz, Continental AG, Hannover, Germany), a laser radar (Model R-Fans 32, 640kHZ, SureStar, Inc., Beijing, China), a smart camera (Model Mobileye EyeQ4, INTC AG, CA, USA), a CANoe analyser (Model VN1640A, Vector, Inc., Stuttgart, Germany), a display monitor and a laptop. The industrial computer communicates with each sensor through the CAN signal, and the industrial computer can be used to deploy the system operating environment and multitarget tracking algorithm. The industrial computer uses the target state obtained by multiple sensors to perform real-time multitarget tracking and multisensor information fusion and outputs the multitarget tracking results to CANoe in the form of CAN signals. CANoe is used to acquire, analyse and store the CAN bus data during the experiment in real time, and the experimental data are analysed by using the CANoe data analysis platform deployed on a laptop computer. In addition, both the experimental and all target vehicles are installed with a inertial integrated navigation system (GNSS/INS) (Model LCA-328T, RION, Inc., Shenzhen, China) for realtime acquisition of the status of each target. The GNSS/INS system offers measurement accuracy at centimetre-level and can provide true relative values to verify the multitarget tracking accuracy before and after multisensor fusion.

The software platform uses the Ubuntu 20.04 operating system. RoboWare Studio and ROS Melodic Morenia are installed, and the relevanted feature packs and function libraries are configured. ROS Topics is used to satisfy the information interaction between sensor nodes and core algorithms to achieve the spatial registration of distributed multisensor systems and the effective deployment of multisensor multitarget tracking algorithms. The construction and integration of the experimental platform are displayed in Fig. 10.

In the real vehicle experiment, a wire-controlled commercial semitrailer tractor equipped with the above experimental platform is employed as the experimental vehicle for tracking multiple target vehicles. In addition, two passenger vehicles equipped with a GNSS/INS in the centre of their roofs are selected as the tracking targets. The camera is positioned centrally at the bottom of the front windshield of the experimental vehicle. The MMW radar and lidar are deployed at the central position surrounded by the front of the

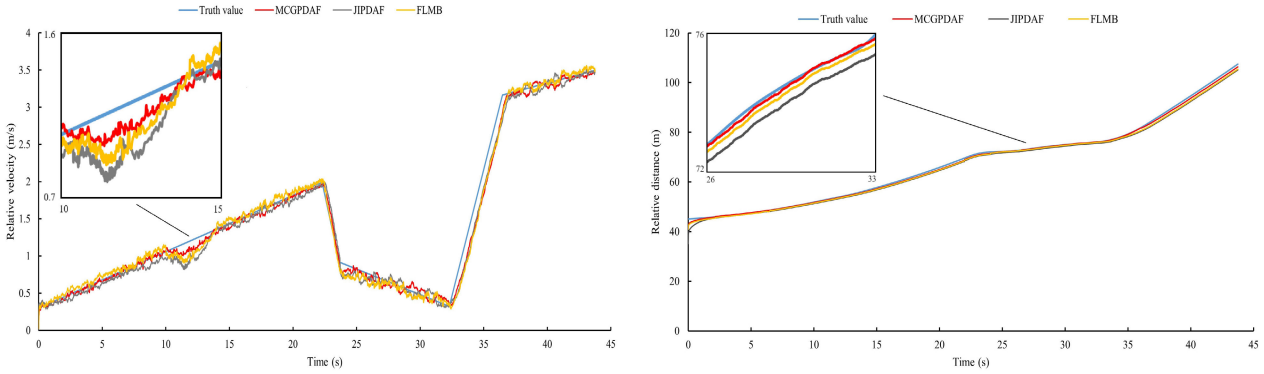

(a) Tracking results of different algorithms on relative velocity

(b) Tracking results of different algorithms on relative distance

FIGURE 7. Tracking results of the relative velocity and relative distance between tracking vehicle T_0 and target vehicle T_1 ($\lambda = 2 \times 10^{-4}$).

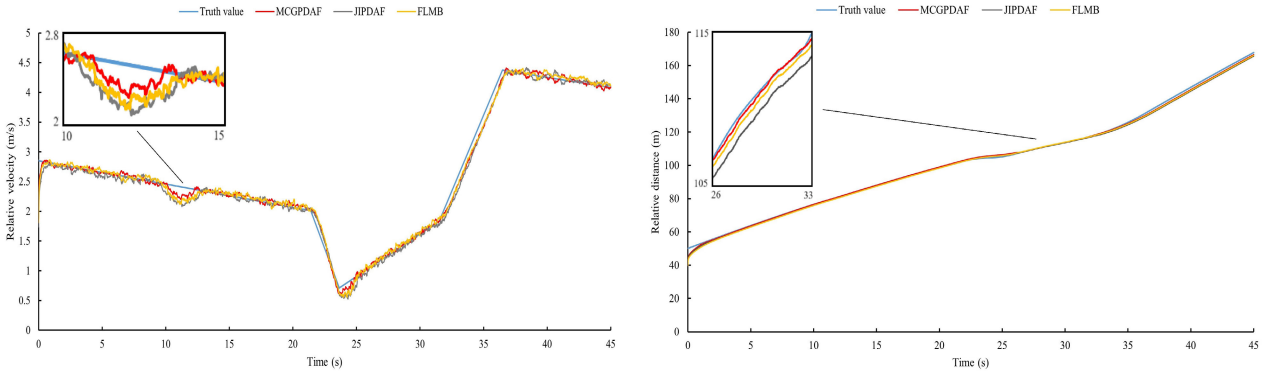

(a) Tracking results of different algorithms on relative velocity

(b) Tracking results of different algorithms on relative distance

FIGURE 8. Tracking results of the relative velocity and relative distance between tracking vehicle T_0 and target vehicle T_2 ($\lambda = 2 \times 10^{-4}$).

TABLE 1. Multitarget tracking accuracy of different algorithms.

Algorithm name	Means of RMSE (Target T1)		Means of MAPE (Target T1)		Means of RMSE (Target T2)		Means of MAPE (Target T2)	
	Relative velocity) (m/s	Relative distance (m)	Relative velocity (%)	Relative distance (%)	Relative velocity) (m/s	Relative distance (m)	Relative velocity (%)	Relative distance (%)
MCGPDAF	0.0824	0.1924	1.3962	1.6837	0.0768	0.1891	1.3125	1.6592
JIPDAF [22]	0.1156	0.2761	1.9865	2.4618	0.1083	0.2679	1.8671	2.3651
FLMB [27]	0.0996	0.2382	1.6893	2.0873	0.0952	0.2318	1.6258	2.0215

experimental vehicle, with the MMW radar positioned 15cm above the lidar in vertical direction. Each sensor and the experimental vehicle are rigidly connected to mitigating any potential impact of sensor jitter on the tracking accuracy during the experiment.

B. PERFORMANCE COMPARISON EXPERIMENT OF MULTITARGET TRACKING ALGORITHMS

To validate the efficacy and performance advantages of the MCGPDAF algorithm proposed in this study across diverse environments, we conducted real-world experiments on single-sensor multitarget tracking. Based on the experimental results, a comparative analysis of tracking performance was conducted between our algorithm and JIPDAF and FLMB algorithms. The experiment employed comprehensive road condition encompassing typical sections and various complex scenarios for multitarget tracking. The driving segments comprised both highways and urban roads in sunny or rainy weather conditions, covering complex scenes such as trees, pedestrians, guardrails, intersections, and multitarget high-speed and low-speed driving. The raw data of multitarget tracking under the above comprehensive road condition

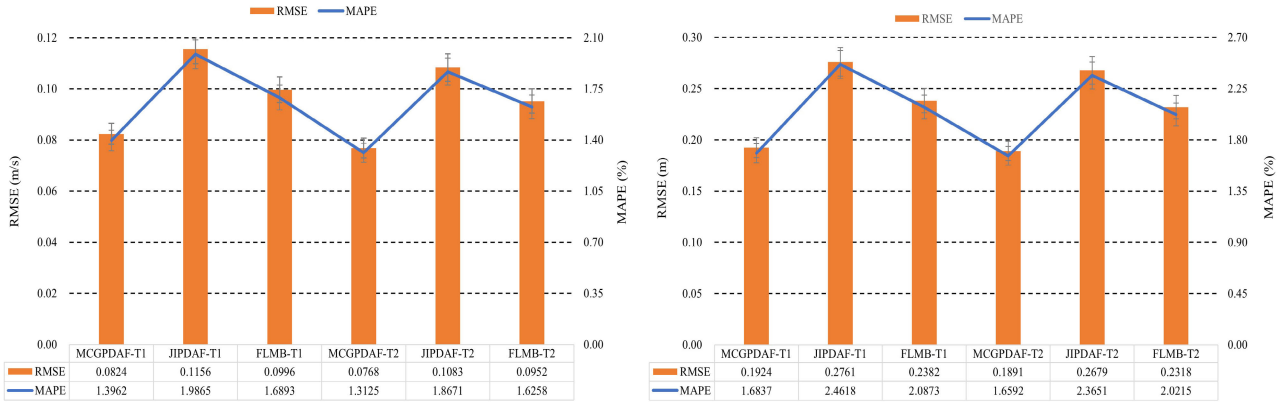

(a) Tracking accuracy of the multitarget relative velocity

(b) Tracking accuracy of the multitarget relative distance

FIGURE 9. Comparison of the RMSE and MAPE results for multitarget tracking via different algorithms.

FIGURE 10. The construction and integration of the experimental platform.

was collected using MMW radar and camera sensors deployed on the experimental vehicle. The comprehensive road condition selected for the experiment encompass a range of intricate real-life scenarios and typical sections, as illustrated in Fig.11. The specific parameters of the millimeter-wave radar sensor are presented in Table 2.

TABLE 2. The parameters of the millimeter-wave radar sensor.

Parameter types	Value
Carrier frequency [GHz]	77
Frame rate [frames /s]	30
Sweep bandwidth [MHz]	500
Max range [m]	170
Max velocity [m/s]	66
Range resolution [m]	0.04
Velocity resolution [m/s]	0.06
Sampling frequency [Hz]	25

The experiment employs the mean accuracy (MOTA) and the average precision (MOTP) of multitarget tracking, and average time (AT) for data association as evaluation metrics to assess the performance of various multitarget tracking algorithms [37]. The MOTA is employed to quantify the accuracy of multitarget data association, while MOTP is utilized to measure the precision of target position estimation. The calculation methods for MOTA and MOTP are outlined below:

$$MOTA = 1 - \frac{FN + FP + IDSW}{GT} \tag{52}$$

$$MOTP = 1 - \frac{\sum_{t,i} d_{t,i}}{\sum_t C_t} \tag{53}$$

where FP and FN represent the total number of false detection and missed detection of the target during the tracking process, respectively, $IDSW$ denotes the cumulative count of incorrect associations between the target and measurements during tracking process, C_t represents the count of accurate matches between the actual position and predicted position of the target at time t, $d_{t,i}$ denotes the Euclidean distance between the actual position and predicted position of the target at time t.

The MCGPDAF, JIPDAF, and FLMB algorithms were deployed on the industrial computer, utilizing the collected raw radar signals served as the experimental data input for the system. Conduct multitarget tracking experiments on road vehicles utilizing the above three tracking algorithms, and subsequently compare the results of multitarget tracking obtained from MMW radar with corresponding raw video tracking data. Finally, perform statistical analysis to evaluate the multitarget association performance and tracking effectiveness of each algorithm. In order to visually demonstrate the multitarget tracking performance of various algorithms in different environments, we conducted experiments on four complex scenarios and typical road sections as depicted in Fig. 11, and recorded the experimental results separately. The experimental results of multitarget tracking under different scenarios and road sections are presented in Table 3.

FIGURE 11. Experimental Scenarios and Road Segment Examples. (Figure a denotes urban roads under clear weather conditions with multitarget, labeled as SR-A; Figure b illustrates urban roads under rainy weather conditions with multitarget, labeled as SR-B; Figure c denotes highways under clear weather conditions with multitarget, labeled as SR-C; Figure d illustrates highways under rainy weather conditions with multitarget, labeled as SR-D.)

TABLE 3. Multitarget tracking performance of each algorithm in various scenarios and road segments.

The name of Scene and road segment	Algorithm name	MOTA (%)	MOTP (%)	AT (s)
SR-A	MCGPDAF	87.63	85.92	0.063
	JIPDAF	68.75	65.31	0.135
	FLMB	76.24	74.59	0.056
SR-B	MCGPDAF	85.72	84.23	0.064
	JIPDAF	66.87	64.18	0.138
	FLMB	75.63	73.69	0.058
SR-C	MCGPDAF	89.34	87.88	0.061
	JIPDAF	71.35	67.43	0.081
	FLMB	78.16	76.27	0.055
SR-D	MCGPDAF	88.05	86.22	0.062
	JIPDAF	69.81	66.07	0.082
	FLMB	77.24	75.36	0.056

According to the experimental results, it can be concluded that the MCGPDAF algorithm exhibits higher multitarget tracking accuracy and offers significant performance advantages across diverse complex environments and road segments. Compared to the JIPDAF and FLMB algorithms, the MOTA of MCGPDAF algorithm improves by 18.49% and 10.87%, respectively, and the MOTP enhances by 20.32% and 11.09%, respectively. In terms of computational efficiency, the average time consumption per association of MCGPDAF algorithm is 0.047 s lower than that of JIPDAF algorithm, albeit it is higher by 0.006 s compared to the FLMB algorithm. The experimental results demonstrate that the MCGPDAF algorithm effectively addressing the complexities and variations of scenes, road sections, and target movements in real-world environments. It has strong robustness and universality during multitarget tracking processes.

In addition, sensitivity analysis experiments of the MCGPDAF algorithm were conducted based on the aforementioned complex scenarios and typical road sections. The experiment was conducted with the position and heading constraint parameters $\Delta d_j^t(k)$, $\Delta\delta_j^t(k)$, and fading factor $\eta(k)$ as the variable parameters of the system. Five periods of multitarget tracking were performed on SR-A class scenarios and road sections depicted in Fig.11, with a tracking duration of 180 seconds for each period. According to the results of multitarget tracking over five periods, we have investigated and analyzed the impact of improvement factors such as constraint parameters $\Delta d_j^t(k)$, $\Delta\delta_j^t(k)$, and fading factor $\eta(k)$

on algorithm performance. The visualization results of the first tracking period of the sensitivity analysis experiment are shown in Fig. 12, and the comprehensive results of the sensitivity analysis experiments for five tracking periods are presented in Table 4.

The experimental results demonstrate that the multi-constraint parameter mechanism of the MCGPDAF algorithm significantly enhances the accuracy of multitarget data association and state estimation. Furthermore, the incorporation of the fading factor has further enhanced the multitarget tracking performance of the MCGPADF algorithm, particularly by enhancing the accuracy of multitarget state estimation. Compared with the GPDAF algorithm, the introduction of constraint parameters $\Delta d_j^t(k)$ and $\Delta \delta_j^t(k)$ improves the MOTA and MOTP of the MCGPDAF algorithm by 17.19% and 14.93%, respectively. Furthermore, the fading factor $\eta(k)$ is introduced to further increase the MOTA and MOTP by 0.93% and 3.36%. In general, the MCGPDAF algorithm demonstrates a slight decrease in computational efficiency compared to the baseline algorithm GPDAF, yet it exhibits significant improvement in overall performance.

TABLE 4. Comprehensive results of the sensitivity analysis experiments.

Parametric variable	MOTA (%)	MOTP (%)	AT (s)
MCGPDAF $\left(\Delta d_j^t(k), \Delta \delta_j^t(k), \eta(k)\right)$	88.27	86.52	0.063
MCGPDAF $\left(\Delta d_j^t(k), \Delta \delta_j^t(k)\right)$	87.34	83.16	0.061
GPDAF (none)	70.15	68.23	0.057

Finally, the computational efficiency of various algorithms in practical applications is compared and analyzed according to the experimental results of the multitarget tracking and sensitivity analysis conducted in complex scenarios and typical road sections. The experimental results demonstrate that the generalized joint event of MCGPDAF algorithm can effective establishment the corresponding relationship between multiple measurements and multiple targets. Compared with the JIPDAF algorithm, MCGPDAF has lower computational complexity, which is particularly advantageous in scenarios with numerous obstacles on urban roads. The MCGPDAF algorithm achieves an average improvement in computational efficiency of 39.01% compared to the JIPDAF algorithm. In comparison with the FLMB algorithm and baseline algorithm GPDAF, the MCGPDAF algorithm experiences an average decrease in computational efficiency of 10.01% and 9.52%, respectively. Although the computational efficiency of the MCGPDAF algorithm is slightly higher than FLMB and GPDAF, the average time consumed for one association of MCGPDAF algorithm (62.5 ms) remains smaller than the output period of each sensor (70 − 100 ms). Therefore, the execution efficiency of the MCGPDAF algorithm adequately satisfies the real-time requirements of multitarget tracking.

C. EXPERIMENTAL AND RESULT ANALYSIS OF MULTITARGET TRACKING WITH MULTISENSOR FUSION

During the real vehicle experiment, the experimental vehicle is utilized to track two target vehicles, T_1 and T_2. The initial relative distances between the experimental vehicle and the target vehicles T_1 and T_2 are 100 m and 80 m, respectively. The three vehicles start at the same time. Targets T_1 and T_2 accelerate to 50 km/h and maintain their speed. After the experimental vehicle accelerates to 60 km/h, the driver gradually slows down and maintains stable tracking considering the distance between the experimental vehicle and the two target vehicles. In Fig. 13, the trajectories of the targets T_1 and T_2 are depicted in the inertial coordinate system, with the driving starting point of the experimental vehicle as the origin. Additionally, the real tracking process and scene from the perspective of the experimental vehicle is showcases in Fig. 14.

During the experiment, each sensor achieves multitarget data association and state estimation based on the MCGPDAF algorithm and then achieves multisensor multitarget state estimation fusion and tracking through target matching and covariance cross fusion. The single-sensor multitarget tracking results based on the MCGPDAF algorithm and multisensor multitarget tracking results based on multisensor perception fusion are obtained synchronously via CANoe. The real vehicle experimental results show the relative distance and relative speed between the experimental vehicle and each target vehicle in the multitarget tracking process (Fig. 15 and Fig. 16) and the corresponding multitarget tracking accuracy results (Table 5 and Fig. 17).

During the real vehicle experiment, multitarget crossing and turning manoeuvres increase the number of measurement outliers in the system, resulting in increased errors in multitarget measurement association and state estimation. The analysis of Fig. 15 and Fig. 16 shows that the multitarget tracking effect of each sensor is ideal, which proves that the MCGPDAF algorithm can effectively restrain the affects of measurement anomalies and the errors of motion estimation model on the precision of multitarget data associations during real vehicle experiments. The effectiveness of the MCGPDAF algorithm is thus further substantiated. Furthermore, compared with the multitarget tracking results of a single sensor, the fusion result obtained by the dynamic multitarget obstacle tracking and monitoring method proposed in this research is closer to the relative true value and has higher multitarget tracking accuracy and better convergence of errors.

Multiple targets are tracked by each sensor via the MCGPDAF algorithm during the real vehicle experiment. Table 5 and Fig. 17 show that the tracking accuracy of lidar is greater than that of MMW radar and camera under the same multitarget tracking algorithm, which is related to the working principle and characteristics of the sensor itself. Multisensor estimation fusion yields superior accuracy in multitarget tracking compared to single-sensor multitarget tracking. The proposed fusion method is used to track the

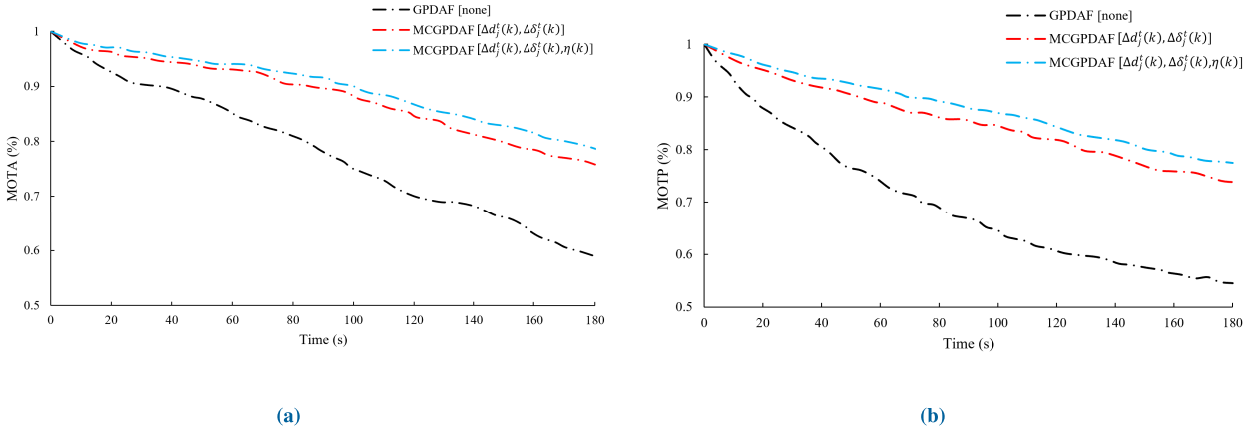

FIGURE 12. Visualization results of the sensitivity analysis experiments ($T = 1$).

TABLE 5. Multisensor multitarget tracking accuracy.

Data sources	Means of RMSE (Target T1)		Means of MAPE (Target T1)		Means of RMSE (Target T2)		Means of MAPE (Target T2)	
	Relative velocity (m/s)	Relative distance (m)	Relative velocity (%)	Relative distance (%)	Relative velocity (m/s)	Relative distance (m)	Relative velocity (%)	Relative distance (%)
Radar	0.1069	0.2439	1.5672	1.9078	0.1129	0.2576	1.6537	2.0369
Lidar	0.0923	0.2105	1.3406	1.6254	0.0937	0.2263	1.3652	1.7364
Camera	0.1235	0.2794	1.8354	2.2026	0.1264	0.2965	1.8739	2.3283
Fusion	0.0758	0.1798	1.1025	1.3785	0.0816	0.1893	1.1867	1.4695

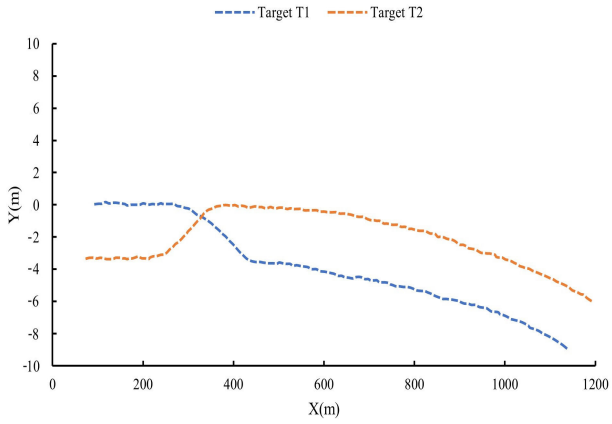

FIGURE 13. Motion trajectories of multiple targets.

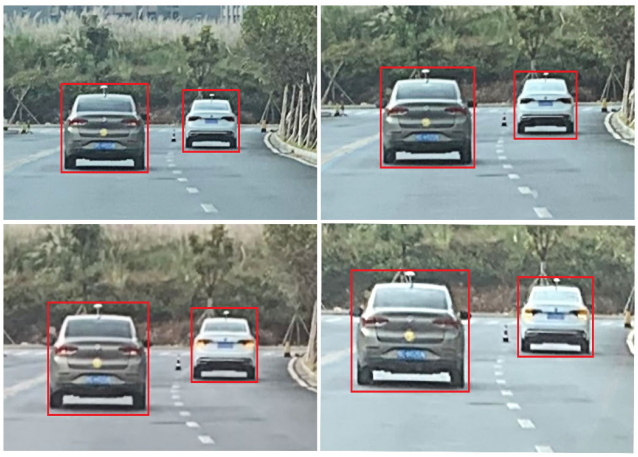

FIGURE 14. Tracking process and scenario of the real vehicle experiment.

relative velocities of targets T_1 and T_2, and the resulting RMSE values are 0.0758 m/s and 0.0816 m/s, respectively; similarly, the MAPE values are 1.1025% and 1.1867%, respectively. The multisensor fusion method put forward in this research is employed to track the relative velocities of targets T_1 and T_2, and the resulting RMSE values are 0.1798 m/s and 0.1893 m/s, while the MAPE values are 1.3785% and 1.4695%, respectively. Compared with the multitarget tracking results for each single sensor, the fusion results obtained by the dynamic multitarget obstacle tracking and monitoring method proposed in this paper have average increases of 26.94% and 25.92% in the RMSE values of the relative speed and relative distance, respectively, and average increases of 27.56% and 26.74% in the MAPE values of the relative speed and relative distance, respectively. In summary, the above experiments and analysis show that the MCGPDAF algorithm can fully utilize its best performance and advantages in the actual multitarget vehicle tracking process. On this basis, the multitarget tracking method of multisensor fusion put forward in this research can further

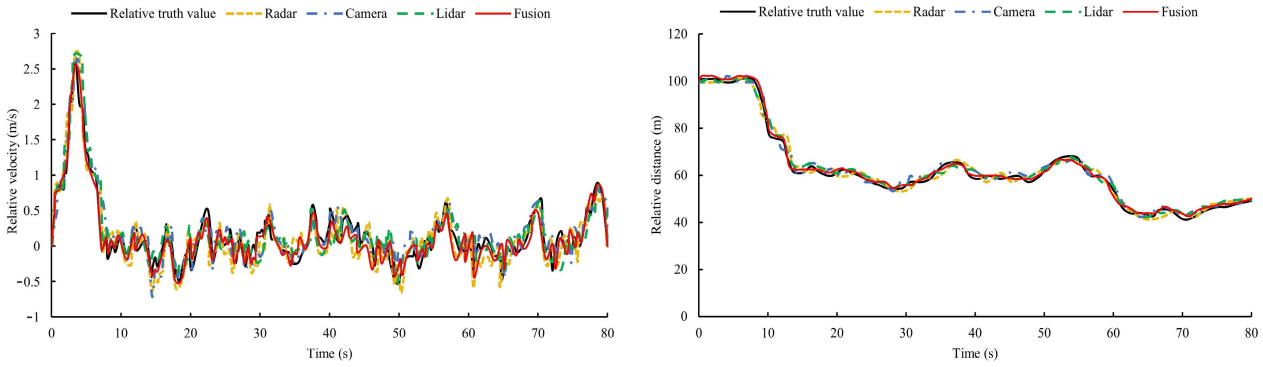

(a) State estimation and fusion results of the relative velocity

(b) State estimation and fusion results of the relative distance

FIGURE 15. Tracking results for the relative velocity and relative distance between the experimental vehicle and target T_1.

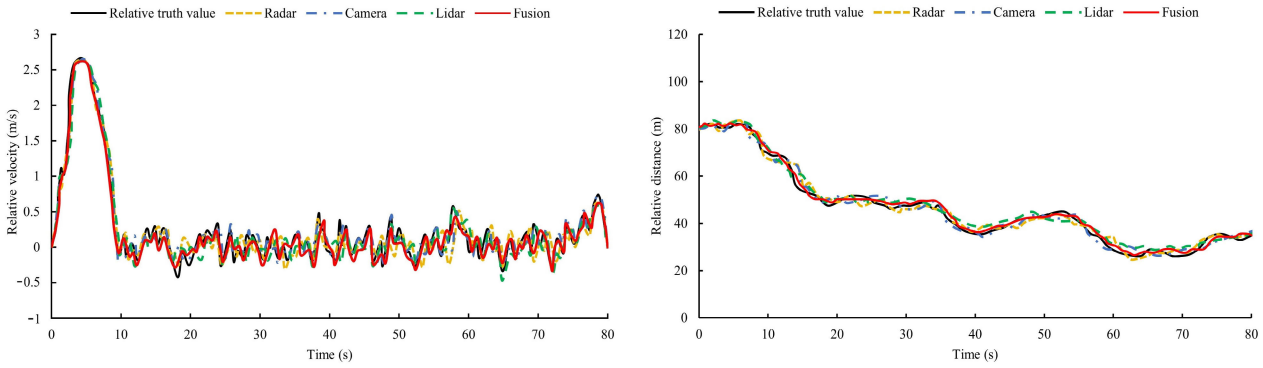

(a) State estimation and fusion results of the relative velocity

(b) State estimation and fusion results of the relative distance

FIGURE 16. Tracking results for the relative velocity and relative distance between the experimental vehicle and target T_2.

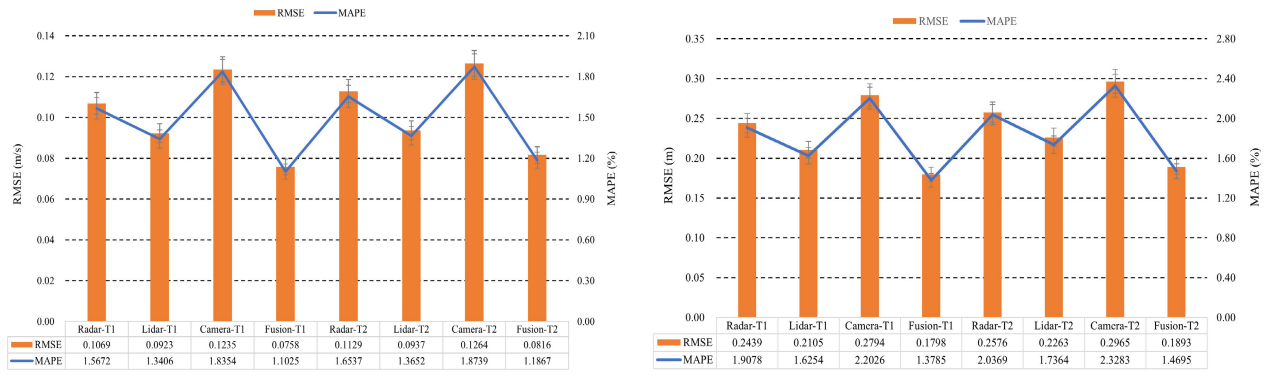

(a) Tracking accuracy of the multitarget relative velocity

(b) Tracking accuracy of the multitarget relative distance

FIGURE 17. Comparison of multitarget tracking accuracy between multisensor fusion and nonfusion.

enhance the tracking performance and accuracy of multitarget vehicle.

In general, the fusion of multiple sensors can further improve the accuracy of multitarget tracking. However, this method requires an increase in hardware costs and still faces challenges and research opportunities in terms of time synchronization among multiple sensors and improvement of sensor perception performance. Therefore, considering that the MCGPDAF algorithm has already demonstrated superior tracking performance, the choice of fusion type and

quantity of sensors can be based on the actual requirements of engineering applications. In future research, the system integration and application scheme with appropriate sensor types and quantities can be further studied based on the algorithm proposed in this paper. This will contribute to balancing hardware costs, multitarget tracking accuracy, and efficiency.

VI. CONCLUSION

Multitarget tracking is an important basis for correct decision-making and precise control of intelligent vehicles. To restrain the interferences of measurement association anomalies and aprior information errors under complex conditions, such as multitarget crossover and large-scale manoeuvring, and to achieve accurate multitarget tracking, a MCGPDAF algorithm is put forward in this research. The MCGPDAF algorithm uses the position and heading information of the dynamic target to construct constraint parameters to calculate the association probability between each effective measurement combination and the target track, enabling the robust association of single-sensor multitarget measurements and accurate tracking in complex environments and working conditions. On this basis, a multitarget tracking and monitoring method based on composite perception fusion is also proposed. The track correlation between multiple sensors and the estimation fusion of multiple target states are obtained by using the correlation sequential track correlation algorithm and the covariance cross fusion algorithm, which further improve the tracking accuracy of the multitarget vehicle. To validate the performance of this multitarget tracking method, both simulation and real vehicle experiments under various environments and roads are conducted. The simulation results reveal that, compared with those of the current advanced algorithms, the RMSE and MAPE of the MCGPDAF algorithm for tracking multitarget state are improved by 23.97% and 24.35% on average. The real vehicle experimental results reveal that, compared with the current advanced algorithms, the MOTA and MOTP of MCGPDAF algorithm improves by 14.68% and 15.71% on average. Moreover, compared with single-sensor multitarget tracking, the RMSE and MAPE of multisensor perception fusion results based on MCGPDAF algorithm are improved by 26.43% and 27.15% on average. The simulation and experimental results underscore that the superior tracking accuracy and generality of the MCGPDAF algorithm, which proves the practicality of the algorithm and architecture displayed in this study.

REFERENCES

[1] M. Cheng, Y. Yan, Y. Han, H. Lei, and C. Deng, "Adaptive machine learning algorithm for human target detection in IoT environment," *Computing*, vol. 106, no. 4, pp. 1139–1150, Apr. 2024.

[2] Y. Liu, Z. Wang, L. Peng, Q. Xu, and K. Li, "A detachable and expansible multisensor data fusion model for perception in level 3 autonomous driving system," *IEEE Trans. Intell. Transp. Syst.*, vol. 24, no. 2, pp. 1814–1827, Feb. 2023.

[3] H. Lian, X. Pei, and X. Guo, "A local environment model based on multi-sensor perception for intelligent vehicles," *IEEE Sensors J.*, vol. 21, no. 14, pp. 15427–15436, Jul. 2021.

[4] Z. Guang-Pu, Z. Ce, Q. Long-Hao, and S. Si-Bo, "Multi-Bernoulli filter for tracking multiple targets using sensor array," *China Ocean Eng.*, vol. 34, no. 2, pp. 245–256, 2020.

[5] B. Khaleghi, A. Khamis, F. O. Karray, and S. N. Razavi, "Multisensor data fusion: A review of the state-of-the-art," *Inf. Fusion*, vol. 14, no. 1, pp. 28–44, 2023.

[6] A. Sharma and S. Chauhan, "Sensor fusion for distributed detection of mobile intruders in surveillance wireless sensor networks," *IEEE Sensors J.*, vol. 20, no. 24, pp. 15224–15231, Dec. 2020.

[7] X. Yan, B. Chen, Y. Zhang, and L. Yu, "Distributed encryption fusion estimation against full eavesdropping," *Automatica*, vol. 153, Jul. 2023, Art. no. 111025.

[8] H. Dai, M. Pollock, and G. Roberts, "Bayesian fusion: Scalable unification of distributed statistical analyses," *J. Roy. Stat. Soc. B, Stat. Methodol.*, vol. 85, no. 1, pp. 84–107, 2021.

[9] Q. Li, C. Zhang, Q. Hu, P. Zhu, H. Fu, and L. Chen, "Stabilizing multispectral pedestrian detection with evidential hybrid fusion," *IEEE Trans. Circuits Syst. Video Technol.*, vol. 34, no. 4, pp. 3017–3029, Apr. 2024.

[10] B. Chen, X. Pei, and Z. Chen, "Research on target detection based on distributed track fusion for intelligent vehicles," *Sensors*, vol. 20, no. 1, p. 56, Dec. 2019.

[11] T. Zhonglin, M. Nadhir Ab Wahab, M. Firdaus Akbar, A. Sufril Azlan Mohamed, M. Halim Mohd Noor, and B. Affendi Rosdi, "SFFSORT multi-object tracking by shallow feature fusion for vehicle counting," *IEEE Access*, vol. 11, pp. 76827–76841, 2023.

[12] Y. Yao, J. Zhao, and L. Wu, "Doppler data association scheme for multi-target tracking in an active sonar system," *Sensors*, vol. 19, no. 9, p. 2003, Apr. 2019.

[13] J. Wang, B. Yang, W. Wang, and Y. Bi, "Multiple-detection multi-target tracking with labelled random finite sets and efficient implementations," *IET Radar, Sonar Navigat.*, vol. 13, no. 2, pp. 272–282, 2019.

[14] K. Echihabi, T. Tsandilas, A. Gogolou, A. Bezerianos, and T. Palpanas, "ProS: Data series progressive k-NN similarity search and classification with probabilistic quality guarantees," *VLDB J.*, vol. 32, no. 7, pp. 763–789, 2023.

[15] W. Guo, Y. Jin, B. Shan, X. Ding, and M. Wang, "Multi-cue multi-hypothesis tracking with re-identification for multi-object tracking," *Multimedia Syst.*, vol. 28, no. 3, pp. 925–937, 2022.

[16] S. A. Memon, I. Ullah, U. Khan, and T. L. Song, "Smoothing linear multi-target tracking using integrated track splitting filter," *Remote Sens.*, vol. 14, no. 5, p. 1289, Mar. 2022.

[17] M. Lucena de Souza, A. Gaspar Guimarães, and E. Leite Pinto, "A novel algorithm for tracking a maneuvering target in clutter," *Digit. Signal Process.*, vol. 126, Jun. 2022, Art. no. 103481.

[18] R. Mahler, "Bayes-optimal tracking of two statistically correlated targets in general clutter," *IET Signal Process.*, vol. 16, no. 2, pp. 1034–1049, 2022.

[19] J. Kim, S. Lee, and H. Kang, "Multitarget tracking with LiDAR and stereo vision based on probabilistic data association fir filter," *J. Elect. Eng. Technol.*, vol. 17, pp. 641–654, Oct. 2022.

[20] B. Liu, R. Tharmarasa, R. Jassemi, D. Brown, and T. Kirubarajan, "Extended target tracking with multipath detections, terrain-constrained motion model and clutter," *IEEE Trans. Intell. Transp. Syst.*, vol. 22, no. 11, pp. 7056–7072, Nov. 2021.

[21] L. Cheng, M. Xue, Y. Wang, Y. Wang, and Y. Bi, "A robust tracking algorithm based on modified generalized probability data association for wireless sensor network," *IEEE Trans. Ind. Electron.*, vol. 69, no. 2, pp. 2136–2146, Feb. 2022.

[22] P. Zhang, J. Yan, L. Ma, Y. Guan, and H. Liu, "An IPDA based target existence assisted Bayesian detector for target tracking in clutter," *Signal Process.*, vol. 205, Apr. 2023, Art. no. 108895.

[23] B. Yu, T. Li, S. Ge, and H. Gu, "Robust CPHD fusion for distributed multitarget tracking using asynchronous sensors," *IEEE Sensors J.*, vol. 22, no. 1, pp. 1030–1040, Jan. 2022.

[24] Á. F. García-Fernández and L. Svensson, "Trajectory PHD and CPHD filters," *IEEE Trans. Signal Process.*, vol. 67, no. 22, pp. 5702–5714, Nov. 2019.

[25] C. Cao and Y. Zhao, "Multi-sensor multi-target tracking with generalized labeled multi-Bernoulli filter based on track-before-detect observation model using Gaussian belief propagation," *Digit. Signal Process.*, vol. 153, Oct. 2024, Art. no. 104618.

[26] Q. Guo, L. Teng, and X. Wu, "Generalized labeled multi-Bernoulli filter with signal features of unknown emitters," *Frontiers Inf. Technol. Electron. Eng.*, vol. 23, pp. 1871–1880, Dec. 2022.
[27] C. Xuan, J. Hongbing, and Z. Yongquan, "Effective implementation and improvement of fast labeled multi-Bernoulli filter," *J. Syst. Eng. Electron.*, vol. 34, no. 3, pp. 661–673, Jun. 2023.
[28] B. Cai, X. Shao, Y. Liu, X. Kong, H. Wang, H. Xu, and W. Ge, "Remaining useful life estimation of structure systems under the influence of multiple causes: Subsea pipelines as a case study," *IEEE Trans. Ind. Electron.*, vol. 67, no. 7, pp. 5737–5747, Jul. 2020.
[29] B. Cai, H. Fan, X. Shao, Y. Liu, G. Liu, Z. Liu, and R. Ji, "Remaining useful life re-prediction methodology based on Wiener process: Subsea Christmas tree system as a case study," *Comput. Ind. Eng.*, vol. 151, Jan. 2021, Art. no. 106983.
[30] S. Atif, S. Khan, and I. Naseem, "Multi-kernel fusion for RBF neural networks," *Neural Process. Lett.*, vol. 55, pp. 1045–1069, Jun. 2023.
[31] X. Zhang, "An optimal data fusion algorithm in the presence of unknown cross covariances," *IEEE Trans. Autom. Control*, vol. 65, no. 3, pp. 1226–1233, Mar. 2020.
[32] C. Quaranta and G. Balzarotti, "Estimation of consistent cross-covariance matrices in a multisensor data fusion," *IEEE Trans. Aerosp. Electron. Syst.*, vol. 58, no. 6, pp. 5456–5469, Dec. 2022.
[33] T. Li, X. Wang, Y. Liang, and Q. Pan, "On arithmetic average fusion and its application for distributed multi-Bernoulli multitarget tracking," *IEEE Trans. Signal Process.*, vol. 68, pp. 2883–2896, 2020.
[34] T. Li and F. Hlawatsch, "A distributed particle-PHD filter using arithmetic-average fusion of Gaussian mixture parameters," *Inf. Fusion*, vol. 73, pp. 111–124, Sep. 2021.
[35] G. Han, F. Liu, and J. Deng, "An adaptive vehicle tracking enhancement algorithm based on fuzzy interacting multiple model robust cubature Kalman filtering," *Circuits, Syst., Signal Process.*, vol. 43, pp. 191–223, Sep. 2023.
[36] W. Ali, Y. Li, M. A. Z. Raja, and N. Ahmed, "Generalized pseudo Bayesian algorithms for tracking of multiple model underwater maneuvering target," *Appl. Acoust.*, vol. 166, Sep. 2020, Art. no. 107345.
[37] S. Han, P. Huang, H. Wang, E. Yu, D. Liu, and X. Pan, "MAT: Motion-aware multi-object tracking," *Neurocomputing*, vol. 476, pp. 75–86, Mar. 2022.

GUOXIN HAN received the B.E. degree in electrical engineering and automation and the M.E. degree in information technology from Heilongjiang Bayi Agricultural University, China, in 2015 and 2019, respectively. He is currently pursuing the Ph.D. degree with Guilin University of Electronic Technology, China. He is also a Lecturer with the School of Computer Science, Zhaoqing University, China. His research interests include signal processing, machine learning, and multi-source information fusion and its application.

FUYUN LIU received the Ph.D. degree in mechanical engineering from Zhejiang University, Hangzhou, China, and the M.E. degree in mechanical engineering from Luoyang Institute of Technology, Luoyang, China. He is currently a Professor with the College of Mechanical and Electrical Engineering, Guilin University of Electronic Technology, China. His research interests include product digital designs, intelligent vehicles, and mechanical kinetics and its application.

HUIQI LIU received the B.E. degree in mechanical design, manufacturing, and automation from Zhejiang University of Water Resources and Electric Power, China, and the M.E. degree in mechanical engineering from the University of Exeter, U.K. She is currently a Laboratory Teacher with the College of Mechanical and Electrical Engineering, Guilin University of Electronic Technology, China. Her research interests include automotive engineering and mechanical and structure designs.

JUCAI DENG received the M.E. degree in mechanical engineering from Guilin University of Electronic Technology, Guilin, China. He is currently a Senior Engineer at Dongfeng Liuzhou Automobile Company Ltd. He is also the Director and the Chief Expert of the Commercial Vehicle Technology Center. His research interests include automotive development project management, commercial vehicle design and development, and noise vibration and harshness.

WEIHUA BAI received the M.E. degree from the School of Computer Science, South China Normal University, in 2006, and the Ph.D. degree from the School of Computer Science and Engineering, South China University of Technology, Guangzhou, China, in 2017. He is currently a Professor with the School of Computer Science, Zhaoqing University, China. His research interests include cloud computing, parallel scheduling, and software architecture. He is a member of China Computer Federation.

KEQIN LI (Fellow, IEEE) is currently a SUNY Distinguished Professor of computer science with the State University of New York at New Paltz, New Paltz, NY, USA. He is also a National Distinguished Professor with Hunan University, China. He has authored or co-authored more than 810 journal articles, book chapters, and refereed conference papers. He holds more than 60 patents announced or authorized by the Chinese National Intellectual Property Administration. His research interests include cloud computing, fog computing and mobile edge computing, energy-efficient computing and communication, embedded systems, cyber-physical systems, heterogeneous computing systems, CPU-GPU hybrid and cooperative computing, machine learning, and intelligent and soft computing. He is an Associate Editor of the *ACM Computing Surveys*. He has served on the editorial boards for IEEE TRANSACTIONS ON PARALLEL AND DISTRIBUTED SYSTEMS, IEEE TRANSACTIONS ON COMPUTERS, IEEE TRANSACTIONS ON CLOUD COMPUTING, IEEE TRANSACTIONS ON SERVICES COMPUTING, and IEEE TRANSACTIONS ON SUSTAINABLE COMPUTING.